Mon. Not. R. Astron. Soc. **000**, 1–?? (2009) Printed 10 May 2016 (MN LATEX style file v2.2)

# Physical conditions and element abundances in SN and GRB host galaxies at different redshifts

M. Contini
*School of Physics and Astronomy, Tel Aviv University, Tel Aviv 69978, Israel*

arXiv:1605.02438v1 [astro-ph.GA] 9 May 2016

10 May 2016

**ABSTRACT**

We compare the physical parameters and the relative abundances calculated throughout supernova (SN) and $\gamma$-ray burst (GRB) host galaxies by the detailed modelling of the spectra. The coupled effect of shocks and radiation from the starburst within the host galaxy is considered. We have found that 1) shock velocities are lower in long period GRB (LGRB) than in SN host galaxies. 2) O/H relative abundances in SN hosts are scattered within a range 8.0 <12+log(O/H)<8.85 but they are close to solar in LGRB hosts. LGRB galaxies hosting Wolf-Rayet (WR) stars have He/H=0.13 in a few objects. 3) The starburst temperatures within a few SN hosts are relatively high ($T_* > 10^5$ K). $T_*$ in LGRB hosts are $\sim$ 3-8 $10^4$K. 4) The H$\alpha$ absolute flux calculated from the emitting clouds of a few SN hosts at 0.1<z<0.3 is sensibly higher than in the other galaxies. H$\alpha$ increases sharply with the ionization parameter $U$. The present analysis suggests that the SN-host symbiosis is stronger than for GRB in terms of activity. The physical and chemical conditions in the GRB host galaxies are similar to those in SB galaxies within a large z range.

**Key words:** radiation mechanisms: general — shock waves — galaxies: high-redshift — galaxies: abundances — supernovae: general — gamma-ray burst: general

## 1 INTRODUCTION

The explosion of a degenerate carbon-oxygen white dwarf is at the origin of Type Ia Supernovae (SN). SN Type Ib and Type Ic which derive from the collapse of massive stars, (see Maoz et al 2014 for a review) were stripped of their H and He envelopes, respectively. SN Type IIn (e.g. Filippenko 1997) which are characterised by the presence of H, show a wide variety of photometric and spectroscopic properties, while hydrogen deficient SN Type I split into Type Ia which show blended iron-group element emission lines, and Type Ib and Type Ic which are characterised by several lines of intermediate elements. SN explosions lead to collisions of the ejecta with the host galaxy medium. A shock propagates in reverse through the circumstellar matter (CSM), while the shock accompanying the ejecta propagates outwards through the host galaxy clouds (Chevalier 1982).

Observational and theoretical evidences indicate that long duration $\gamma$-ray bursts (LGRB) originate from the death of very massive stars (e.g. Paczynski 1998), they are flashes of cosmic high energy ($\sim$1 keV $-$ 10 GeV) photons (Fishman & Meegan 1995) and explode in star forming galaxies. LGRB and their afterglows are associated with broad lined SN Ic (e.g. Hjorth et al 2003, Stanek et al 2003). They provide information about star-forming galaxies at high z (e.g. Krühler et al 2015, Blanchard et al 2015 and references therein). LGRB host galaxies are moderately star forming (SFR $\sim$ 1-10$M_\odot$ yr$^{-1}$), with stellar masses of $\sim$ 1-5 $10^9 M_\odot$ and high specific star formation rates (Fruchter et al 2006, Savaglio et al 2009). Moreover, they reveal morphology, star forming rates and burst energetics and location relatively to the galaxy centres (Castro-Tirado et al 2001). Sollerman et al (2005) investigating low redshift (z< 0.2) GRB galaxy hosts through spectra which include the HeI 5876 line, concluded that they are star-forming galaxies (L< $L_\odot$ ) with relatively low metallicity. Helium lines are significant for GRB as well as for SN Type Ic relatively to Wolf-Rayet (WR) stars, which could be considered as LGRB progenitors, depending on metallicity (Han et al 2010).

Short duration GRB (SGRB) last less than 2s, while LGRB have longer duration (Kouveliotou et al 1993). Short bursts have significantly fainter afterglows. Their properties are known from their association with the host galaxies (Fong et al. 2013). However, Fong et al could not find a trend linking GRB duration and host type. The lack of an associated supernova and their link to a heterogeneous sample of host galaxies (e.g. Kann et al. 2011) is consistent with a compact binary merger origin (Rosswog et al. 2003), such

© 2009 RAS

as neutron stars or black holes. de Ugarte Postigo (2012) suggested that the merger is not associated with the galaxy star-forming region bulk, but it occurs in dense regions.

In this paper we refer to the narrow line-emission spectra from SN and GRB host galaxies. In SN hosts the spectra are emitted downstream of shock fronts which decelerate colliding with high density clouds. The line ratios account for the physical conditions of the gaseous clouds, for the photoionization flux from the starburst (SB) throughout the host and for the progenitor composition. The spectra seen in GRB hosts originate in star-forming regions, probing the conditions of the gas. SN and GRB are generally analysed by their light curves, whereas the host galaxy properties are investigated by the continuum spectral energy distribution (SED) in the different wavelength domains and by the line spectra. Spectroscopic data provide a full physical and chemical picture for local galaxies. At high redshifts the data are reduced to a few significant lines, but the surveys contain hundreds of objects. Therefore, in order to obtain the O/H metallicity, O/H are calculated by the "direct methods" (see e.g. Modjaz et al 2008). The data are also compared with diagnostic diagrams calculated for general cases. On the other hand, the detailed modelling of the spectra, which is currently used to interpret local galaxy spectra, cannot be always adopted for high z objects, if the models are not constrained enough, e.g. by the lack of the auroral line [OIII]4363 (see Contini 2014a), one of the H lines such as H$\beta$ , H$\alpha$ (H$\gamma$ is not always observed), He lines and others. This leads in particular to the ambiguous identification of the gas photoionizing and heating sources (AGN, SB and/or shocks).

In the following we revisit the emission spectra from the host galaxies of super-luminous SN (SLSN) presented by the Leloudas et al (2015) survey, of different SN types by Sanders et al (2012), of broad lined SN Type Ic by Modjaz et al (2008), of the LGRB hosts from the surveys of Krühler et al, Savaglio et al (2009), Sollerman et al (2005), Castro-Tirado et al (2001), Graham & Fruchter (2013), Levesque et al (2010), Vergani et al (2011), Piranomonte et al (2015), the LGRB line and continuum spectra with WR features from the Han et al (2010) survey and the SGRB line spectra from de Ugarte Postigo et al (2014), Cucchiara et al (2013) and Soderberg et al (2006). We have selected the spectra suitable to constrain the models. The code SUMA[1] which simulates the physical conditions in a gaseous cloud under the coupled effect of photoionization from a primary radiation source and shocks was adopted to calculate the spectra. The line and continuum emission from the gas are calculated consistently with dust-reprocessed radiation in a plane-parallel geometry. The input parameters refer to both the shock and the photoionization source. We obtain the physical characteristics of the different host galaxies reproducing by the calculations the observed line ratios of each object, i.e. the photoionization source intensity flux, its frequency distribution (AGN or SB) and in the SB case the effective temperature and ionization parameter. Moreover, we obtain the shock velocity, the preshock density, the geometrical thickness of the gaseous clouds and the element abundances throughout the host galaxy.

[1] http://wise-obs.tau.ac.il/∼marcel/suma/index.htm

In the following, we present new results and compare them with those of previous investigations, in particular about the element abundances at relatively high redshifts, because metallicity is one of the fundamental parameters which affects the evolution of massive stars (Piranomonte et al, Sollerman et al, etc). In Sect. 2 we briefly comment about modelling approaches. In Sect. 3 we present the modelling of the galaxy hosts and in Sect. 4 we discuss the results regarding the SFR connection with the different physical parameters and element abundances. Concluding remarks follow in Sect. 5.

## 2 MODELLING APPROACH

The code calculates the emission line and continuum flux from a cloud of gas (and dust), independently from the number of the observed lines. The calculated line wavelengths range from far-UV to far-IR. We do not report in the tables the calculated lines which cannot be compared with the data. We refer only to spectra emitted from the SN and GRB host galaxies where the different shock and photoionization events occur. Detailed modelling by the codes e.g. CLOUDY, MAPPINGS, etc., that were assembled following the observations of spectra rich in number of lines from different elements and in different ionization stages, is generally disregarded for high z galaxies, because the observed lines are few, while hundreds of galaxies are observed in each survey. Galaxies at high redshifts often originate from mergers and show a disturbed hydrodynamic structure. Collisional phenomena are critical in the calculation of the spectra adopting models based on the coupled effect of photoionization and shocks. We suggest that they are the closest approximation to the complex structure of the emitting gas and they are therefore suitable to SN and GRB host galaxies.

Different results derive from the different interpretation methods. Anderson et al (2016) claim that emission line diagnostics are separated in two groups. Empirical methods, using the [OIII] 5007/4363 ratio to estimate the emitting gas temperature, calculate the O/H relative abundance directly from the oxygen line ratios to H$\beta$ . The second group compares the observed line ratios with those predicted by photoionization/stellar population synthesis models. Our approach is different. A comparison between the results obtained by the "direct methods" and by the detailed modelling adopting SUMA was presented by Contini (2014a) who suggested that the relative abundances obtained by direct methods are lower limits, because a constant temperature is adopted throughout all the galaxy. It is well known (Williams 1967) that the gas recombines following the cooling rate by free-free, free-bound and line emission in the regions farther from the radiation source and (Cox 1972) following the cooling rate downstream of shock fronts. Therefore, regions of low temperature and density in the galaxy should be considered. The line fluxes are calculated multiplying the fractional abundance of the corresponding ions by the element abundance and integrating throughout the galaxy. The fractional abundance of certain ions (e.g. $O^{++}/O$), considering gas recombination, is lower than the fractional abundance calculated by an homogeneous temperature adapted to the [OIII]5007/4363 line ratio. So, to

reproduce e.g. [OIII]/H$\beta$ a relatively high O/H is adopted. Moreover, all the line ratios in each observed spectrum are reproduced by the same model.

Most of the spectral observations of single high redshift galaxies cover the entire object. Interpreting the average spectra by models used to calculate the parameters in the different regions of a single local galaxy, we reach approximated or even distorted information. For instance, the Galaxy is filled with star clusters, colliding clouds of dust and gas heated and ionized by the flux from an active galactic nucleus (AGN), from SB, SN, etc. Turbulence leads to fragmented gas clouds. The SN remnants (SNR) throughout the ISM reveal different physical conditions and element abundances, e.g. the higher than solar (see Table 1) He/H ∼0.4 in the Crab Nebula filaments (Williams 1967, Contini et al. 1977), the depletion of the heavy elements in the Cygnus Loop (Contini & Shaviv 1980), the different kinds of H, He and N rich flocculi or O and S rich knots (Contini 1987) and other filaments (Fesen & Milisavljevic 2015) in Cassiopeia A, the dusty clouds showing higher than solar N/H in the Kepler SNR (Contini 2004), etc. The emitting clouds surrounding the explosion site are compressed, heated and ionized by the expanding shock which blends with the ISM at large distances. Shifting, for instance, the Galaxy complex to a high redshift and analysing the average spectrum observed at Earth (old position), the single region characteristic parameters would result smoothed and averaged.

The rich spectra observed from local galaxies allow to assemble a multi-cloud model taking into consideration many different clouds within the galaxy (e.g. Rodriguez-Ardila et al 2005). Actually, for high z objects, the observed spectra cover the entire galaxy so, we select for each object the model best fitting the line ratios of a prototype cloud which should prevail throughout the galaxy.

### 2.1 The calculation code

By SUMA, the calculations start at the shock front where the gas is compressed and thermalized adiabatically, reaching the maximum temperature in the immediate post-shock region ($T(K) \sim 1.5\times10^5/(V_s/100$ km s$^{-1})^2$, where $V_s$ is the shock velocity). T decreases downstream following the cooling rate. This region is cut into a maximum of 300 plane-parallel slabs with different geometrical widths, which are determined automatically, in order to follow smoothly the temperature gradient.

The input parameters such as the shock velocity $V_s$ , the atomic preshock density $n_0$, the preshock magnetic field $B_0$, define the hydrodynamical field. They are used in the calculation of the Rankine-Hugoniot equations at the shock front and downstream. They are combined in the compression equation which is resolved throughout each slab of gas in order to obtain the density profile downstream. The input parameters that represent the primary radiation field for a SB are the effective temperature $T_*$ and the ionization parameter $U$. For an AGN, the primary radiation is the power-law radiation flux from the active center $F$ in number of photons cm$^{-2}$ s$^{-1}$ eV$^{-1}$ at the Lyman limit and spectral indices $\alpha_{UV}$=-1.5 and $\alpha_X$=-0.7. The secondary diffuse radiation emitted from the slabs of gas heated by the shocks is also considered. Primary and secondary radiations are calculated by radiation transfer throughout the slabs downstream. The dust-to-gas ratio ($d/g$) and the abundances of He, C, N, O, Ne, Mg, Si, S, A, Fe, relative to H, are also accounted for. They affect the calculation of the cooling rate. The input parameters ($V_s$ , $n_0$, $T_*$ , $U$, $D$, relative abundances, etc) which define a model, are the most significant ones in order to represent the conditions of the gas within a specific object clouds. Hundreds of other parameters are considered in the calculations e.g. the recombination coefficients for each ion of each element, the ionization cross sections etc.

Briefly,

1) an initial input parameter set is adopted on the basis of the galaxy observations;

2) the code calculates the density in the slab of gas downstream by the compression equation,

3) the fractional abundances of the ions from each level for each element,

4) line emission, free-free and free - bound emission flux;

5) the temperature of the gas in the slab is recalculated by thermal balancing or the enthalpy equation;

6) the optical depth of the slab and the primary and secondary fluxes are calculated;

7) the parameters found in slab i are adopted as initial conditions in slab i+1;

8) integrating on the line intensity increments calculated in each slab, the absolute flux of each line is obtained at the nebula (the same for the bremsstrahlung);

9) the line ratios to a certain line (in the present case H$\beta$ ) are calculated.

### 2.2 Method of analysis

In the modelling process we calculate grids of models which approximately reproduce the observed line ratios. We start adopting solar abundances as a first trial (Allen 1976, Table 1). We vary the input parameters until a satisfactory fit to 'all' the observed line ratios is obtained consistently. Each line has a different strength which translates in different precision by the fitting process. A minimum number of significant lines (e.g [OIII] 5007+, [OII]3727+, [OIII]4363, [NII], H$\beta$ , H$\alpha$ ) is necessary to constrain the model but the number of the observed lines does not interfere with the modelling process. Each model calculates more than 200 line (and continuum) fluxes from far-UV to far-IR. We deal with line ratios to avoid distance and morphological effects. We start referring to line ratios of the same element (e.g. [OIII]/[OII], HeII/HeI) because they depend on the physical conditions of the gas. For all models $B_0=10^{-4}$Gauss is adopted. The models are initially constrained by the observed FWHM of the line profiles (when available) which are roughly related with the velocity field and can give a first hint to the shock velocity. In a single galaxy, different emitting regions can be directly recognized from complex FWHM. This determines whether a pluri-cloud model should be considered.

Then, the grids are completed by comparing calculated with observed line ratios to H$\beta$ (e.g. [OIII]/H$\beta$ ), in order to obtain the relative abundances of the different elements. If all the line ratios to H of a single element are higher (or lower) than the observed ones, the relative abundance to H of that element is changed. The abundances of strong

**Table 1.** The solar element abundances

| element | Allen (1976) | Anders & Grevesse (1989) | Asplund et al. (2009) |
|---|---|---|---|
| H | 12 | 12 | 12 |
| He | 11 | 11 | 11 |
| C | 8.52 | 8.56 | 8.43 |
| N | 7.96 | 8.05 | 7.83 |
| O | 8.82 | 8.93 | 8.69 |
| Ne | 8. | 8.09 | 7.93 |
| Mg | 7.4 | 7.58 | 7.6 |
| Si | 7.52 | 7.55 | 7.51 |
| S | 7.2 | 7.21 | 7.12 |
| Cl | 5.6 | 5.5 | 5.5 |
| Ar | 6.52 | 6.56 | 6.4 |
| Fe | 7.5 | 7.67 | 7.5 |

coolants (e.g. He, C, O,) affect the cooling rate (by line emission) of the gas in the recombination zone. Consequently, by increasing or reducing one element abundance, all the calculated line ratios change and even if we have already reached a satisfactory fit for most of the line ratios, the whole modelling process is restarted until all the calculated line ratios are well tuned. A perfect fit is not realistic because the observed data have errors, both random and systematic. The uncertainty in the calculation is due to the atomic parameters (within 10 %) which are often updated. The strongest lines (e.g. [OIII]5007) are reproduced by $< 10\%$, the weakest (e.g. [OIII]4363) by $\sim 50$ %. The calculation code and our modelling method are described by Contini (2014a, 2015 and references therein).

Different grids of models are calculated for different galaxy types. Dealing with spectra of high z objects, which contain mainly oxygen lines, a first hint about the model is given by [OIII]/[OII], which does not depend on O/H, and from [OIII]/H$\beta$ and [OII]/H$\beta$ which depend on both the physical conditions and O/H. The ionization parameter $U$ which represents the ratio between the number of photons from the SB in the host and the number of electrons in the cloud of gas reached by the radiation flux, links the photoionization source with the galaxy ISM properties. Model degeneracy between $T_*$ and $U$ is only apparent. For instance, a higher $T_*$ increases both the [OIII]/H$\beta$ and [OIII]/H$\beta$ line ratios but a higher $U$ not always yields a higher [OII]/H$\beta$ . Line ratios to H$\beta$ in the optical range, which are strong enough to be observed, are shown as function of $U$ (top diagram) and $T_*$ (bottom diagram) in Fig. 1. The chosen ranges are $10^{-3} \leqslant U \leqslant 1$. and $10^4 \leqslant T_* \leqslant 5.10^5$ K (Contini 2015 and references therein). Such diagrams suggest how to reproduce the observed spectra.

### 2.3 The density, [SII] and [NII] lines

The gas density n is a crucial parameter in models accounting for the shocks. In each cloud, n reaches its upper limit downstream and remains nearly constant, while the electron density $n_e$ decreases following recombination. Recall that n is linked with $n_0$ by compression downstream ($n/n_0$) which ranges between $< 10$ and $> 100$, depending on $V_s$ and $B_0$. A high density, increasing the cooling rate, speeds up the recombination process of the gas, enhancing the low ionization level lines. Each line comes from a region of gas at a different electron density and temperature, depending on the ionization level and the atomic parameters characteristic of the ion.

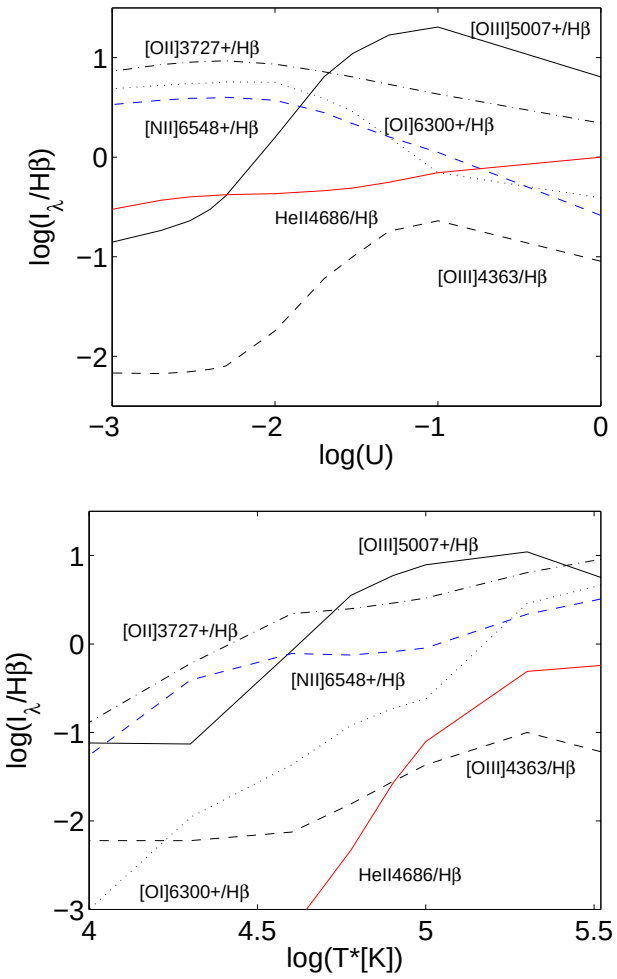


**Figure 1.** Top diagram. The line ratios to H$\beta$ calculated as function of $U$ ($T_*$ =2 $10^5$ K). Bottom diagram. The line ratios to H$\beta$ calculated as function of $T_*$ ($U$=0.03).

The density n is roughly revealed by the [SII]6716/6731 doublet ratio. The [SII] lines are also characterised by a relatively low critical density for collisional deexcitation. In some cases the [SII]6716/6731 line ratio varies from >1 to <1 throughout a relatively small region downstream. In fact the [SII] line ratios depend on both the electron temperature and density of the emitting gas (Osterbrock 1974, fig. 5.3) which, in models accounting for the shocks, are far from constant throughout the clouds. So, even sophisticated calculations which reproduce approximately the highly inhomogeneous conditions of the gas, lead to some discrepancies between the calculated and observed line ratios. So [SII]/H$\beta$ ratios do not reproduce the observations with the required precision. Unfortunately, there are no data for S lines from higher ionization level, which could indicate whether the choice of the model is misleading or different relative abundances should be adopted. Recall that sulphur can be easily de-

pleted from the gaseous phase and trapped into dust grains and molecules. We consider that the [SII]/H$\beta$ line ratios are indicative of the S/H relative abundance.

The same is valid for the [NII] lines. The observations do not contain any other strong line of N, which could confirm whether the gap between the calculated and the observed [NII]/H$\beta$ line ratios can be resolved by changing the N/H relative abundance or the other input physical parameters. Notice that [NII] lines come from the same region of the gas that emits the [OII] lines due to charge exchange reaction between $O^+$, $N^+$ and $H^+$. [OII]/H$\beta$ line ratios depend on the physical parameters and are constrained by [OIII]/H$\beta$ , so the [NII]/H$\beta$ line ratios can easily show abnormal N/H relative abundances. Nitrogen is less abundant than other elements e.g. oxygen, neon, etc., therefore it is not a strong coolant, namely, does not affect strongly the cooling rate of the gas downstream. Changing N/H, the [NII]/H$\beta$ line ratios accordingly change, but the other line ratios are not modified.

### 2.4 O/H and the [OIII] 4363 line

O/H relative abundances calculated by detailed modelling are generally higher than those calculated by the "direct methods". In fact, oxygen is a strong coolant which shapes the temperature, density profiles and the relative distribution of the different ions throughout the host clouds. The contribution from slabs of gas to a line can be low in regions where the gas conditions are less adapted to a high ion fractional abundance. A high element abundance compensates the gap between the calculated and observed line intensity. By the "direct methods" the regions of gas with temperatures and densities less adapted to a line are not considered and the element abundances are calculated directly considering the most appropriated conditions for the ion.

A higher O/H not always yields higher [OIII]/H$\beta$ , [OII]/H$\beta$ and [OI]/H$\beta$ by the same factor, sometimes it even leads to opposite trends, depending on the set of all the input parameters. The [OIII]4363 line depends on the gas temperature and density, constraining the model. The final choice of a model is dictated by [OIII]4363/H$\beta$ (when observed, see Contini 2016) that is calculated consistently with [OIII]5007+/H$\beta$ and [OII]/H$\beta$ . However, this line is generally weak. Its role in modelling the spectra was discussed by Contini (2014a).

## 3 COMPARISON OF OBSERVED WITH CALCULATED SPECTRA

We have gathered the spectra emitted from SN and GRB host galaxies. Modelling results of selected objects are shown in the following.

### 3.1 Leloudas et al (2015) SN galaxy host survey

Leloudas et al (2015) present the spectra from the host galaxies of super luminous SN (SLSN). They are very bright explosions which mostly occur in faint dwarf galaxies. The subtypes SLSNI and SLSNR are H poor and they are distinguished by their light curve evolution. SLSNII are H rich. Leloudas et al (2015) refer to Extreme Emission Line Galaxies (EELG) observations. For spectroscopy they used FORS2 and X shooter on the VLT, OSIRIS on the GTC and IMACS on Magellan. Narrow lines originate from the host galaxy, downstream of the shock produced by collision of the fast moving ejecta with the CSM (see Leloudas et al 2015 and references therein).

We report in Table 2 the data presented by Leloudas et al (2015) in their table B1. For each galaxy the observed line ratios are followed in the two next rows by the best fitting results calculated by shock dominated (SD) models (ml1-ml26) and radiation dominated (RD) models (mll1-mll26) which account for the photoionization flux from the SB + shocks, respectively. In Table 2, columns 8-15, the model input parameters are reported. The SD models (ml1-ml26), which best reproduce the [OII]/H$\beta$ and [OIII]5007+/H$\beta$ line ratios (the + indicates that the doublet is summed) show relatively high shock velocities (except for SN 1999as and SN 1999bd). SD models are presented for all the objects even if a broad component was observed only in the H$\alpha$ and [OIII] line profiles of the PTF11dsf galaxy. This broad component can be attributed to strong outflows of SN winds (Leloudas et al) or from SB star outbursts (Contini 2015). The relatively low velocities of RD models refer to the encounter of the SN outflowing shock with the ISM clouds. The shock velocities and pre-shock densities calculated by RD models are in average similar to those in the proximity of SB clouds (Contini 2015 and references therein). The results of absolute H$\beta$ fluxes (in Table 2, col. 11) calculated for SD models show that the intensity of the line fluxes are lower than those calculated by coupled photoionization and shock by factors between 10 and 1000. Therefore the contribution of high velocity clouds can be hardly distinguished from the underlying noise of the spectra. SD models overpredict the observed [OIII] 4363/H$\beta$ ratios by factors >3. Therefore, RD models are more appropriated. Table 2 results confirm that SN generally occur in SB galaxies and show that some star temperatures are approaching those characteristic of outburst (see Contini 2014b). The temperatures of a few SLSNI and SLSNR host SB are even higher than those found in galaxies with activity at relatively high z. We associate the activity in galaxies ( van Dokkum et al. 2005) to an AGN, a SB, and to shocks on the basis of a strong wind throughout the galaxy, while we refer to quiescent galaxies (Kriek et al. 2009) because emitting weak lines. Those imply a low luminosity AGN and a low star formation rate (SFR = 1 - 3 $M_\odot$ $yr^{-1}$) compared with models of stellar population synthesis SEDs. Contini (2014b) claims that activity is connected with a high SB temperature ($T_* > 10^5$K). The O/H relative abundances are scattered between O/H = $10^{-4}$ and 7.1 $10^{-4}$ (we refer to O/H solar = 6.6 $10^{-4}$ by Allen 1976 in Table 1). N/H are generally lower than solar ($10^{-4}$) by factors of 5-20. The geometrical thickness of the emitting clouds drops from $D \leqslant 30$ pc for galaxies at z$\geqslant$0.3 to $\leqslant$0.3 pc at lower z. In general the shocks accompanying turbulence in the SB lead to fragmentation of matter and to different cloud thickness within a large range.

### 3.2 Sanders et al (2012) SN host galaxy survey

Sanders et al presented the spectroscopic observations of a relatively large sample of different SN type host galaxies at

0.01<z<0.15. The authors were particularly interested in the relative abundances of significant elements. The results of their investigation show rather low metallicities. They were obtained by different methods which are well described in their text. These methods which refer mainly to the oxygen lines cannot provide a consistent representation of the physical properties of the emitting gas such as to explain all the line ratios reported by each galaxy spectrum. Therefore, we have revisited their spectra by detailed modelling (msnd1-msnd24) in order to compare the results and in particular, to provide a more detailed representation of the physical conditions throughout the emitting gaseous clouds. The results of modelling are presented in Table 3. We constrain the models by the weakness of the [OIII]4363 line. These spectra are well reproduced by clouds of gas propagating outwards from the SB (the photoionizing source), while the spectra corresponding to relatively high [OIII]4363/H$\beta$ ($\geqslant$ 0.1) are reproduced by clouds propagating inward towards the SB. In the latter case the radiation flux reaches the shock front of the cloud, in the former case it reaches the edge opposite to the shock front.

To better understand this result we present in Fig. 2 the profile of the electron temperature, electron density and fractional abundances of significant ions throughout the clouds for models msnd15 and msnd15-0 corresponding to outflow and to inflow, respectively. In the outflow case (top diagrams) the emitting cloud is divided into two halves represented by the left and right diagrams. The left diagrams show the region close to the shock front and the distance from the shock front on the X-axis scale is logarithmic. The right diagrams show the conditions downstream far from the shock front, close to the edge reached by the photoionization flux which is opposite to the shock front. The distance from the illuminated edge is given by a reverse logarithmic X-axis scale. The inflow case is represented by the bottom diagram. Fig. 2 diagrams reveal why, compared with Sanders et al results, the metallicities calculated by detailed modelling (Table 3) are generally higher than those deduced by different methods. In the outflow case, the $O^{++}/O$ fractional abundance is very low throughout more than half of the geometrical width of the cloud, therefore to obtain relative high [OIII]4363/H$\beta$ a relatively high O/H is adopted (Sect. 2.4). In the inflow case, $O^{++}/O$ is nearly constant and corresponds to T$\sim 10^4$K, so a relatively low O/H= 4 $10^{-4}$ nicely fits the observed line ratio. Outflow is more suitable to the clouds in SB environments. Inflow in few cases can be justified by the turbulent regime created by shocks throughout SB regions.

### 3.3 Modjaz et al (2008) broad-lined TypeIc SN host galaxies

The element abundances in the host galaxies are a basic issue to understand the characteristics of local and high redshift SN and GRB phenomena. Modjaz et al (2008) presented observations of 12 hosts of broad lined Type Ic at z<0.14 with no observed GRB and derived host galaxy central metallicities (O/H) and metallicities at the SN positions by strong-line diagnostics. Comparing their results with those of five nearby SN-GRB hosts, they found that broad lined SN Ic without GRBs show higher metallicity environments.

The new spectra presented by Modjaz et al are rich of lines which permit the detailed modelling of the line ratios. We have revisited Modjaz et al spectra. The host-galaxy observed emission line-fluxes are given in their tables 4 and 5 measured in the galaxy centre and in the SN positions different from centre, respectively. We present in Tables 4 and 5 the modelling (models mM1-mM8) of line ratios to H$\beta$ (corrected for extinction, Osterbrock 1974). The results reproduce the strong line data within 10%. The observed sulphur doublet 6717/6731 is >1 which would correspond to a very low density ($n_e \leqslant 10$ cm$^{-3}$, adopting $T_e=10^4$K, Osterbrock 1974, fig. 5.3). Such densities are low compared to those found in SN and GRB host galaxy emitting clouds. We refer to preshock densities of $\sim$ 100 cm$^{-3}$, which lead to the satisfactory fit of all the other line ratios. This ambiguity is discussed in Sect. 2.3 and it is probably due to the continuum subtraction.

The 12+(O/H) relative abundances which result from our modelling range between 8.79 and 8.66 in the central galaxy regions and between 8.82 and 8.75 at the SN positions different from the galaxy centre. Modjaz et al results range between a maximum of 9.15 and a minimum of 8.24 with different methods and for different galaxies in the centre and between 9.08 and 8.38 in the SN position out of centre.

### 3.4 Krühler et al (2015) LGRB host galaxy survey

Krühler et al investigate the physical conditions of LGRB host galaxies by recent observations of 90 objects. Long period GRB are connected with core-collapse of progenitors of SN of Type 1c. Krühler et al claim that a GRB explosion represents a very rare endpoint of stellar evolution. They present VLT/X-shooter emission lines of GRB-selected galaxies at 0.1< z< 3.6 and analyse the correlation between the host physical properties and element abundances. We revisited the spectra by the detailed modelling of the line ratios, using models which account consistently for photoionization from an SB + shocks. The spectra lacking the data of some significant lines were excluded because unable to constrain the models. In Table 6 we present the results of modelling. The line ratios have been reddening corrected. The observed FWHM are calculated by $\sigma = \sqrt{FWHM^2 - \Delta V^2}/2\sqrt{2ln2}$, where $\Delta$V$\sim$ 35 km s$^{-1}$, as given by Krühler et al. They are used to constrain $V_s$ . In Table 6, for each observed spectrum, the corrected line ratios are followed in the next row by model results (mk1-mk52). The 090201 spectrum, which shows particularly high gas velocities (400 km s$^{-1}$), could be reproduced by three different models, SD, SB and AGN dominated. The H$\beta$ flux calculated by the AGN model is definitively higher than those calculated by the other models, suggesting that an AGN could be present in the host galaxy. Compared with the models for SLSN hosts, long GRB hosts in the same z range show in general very low ionization parameters $U$, indicating relatively high dilution of the radiation flux due to a large distance R of the emitting gas from the photoionization source. The flux $F$ from the SB stars and the ionization parameter $U$ are combined by $F(r/R)^2 = Unc$, where r is the radius of the star, R the distance to the emitting nebula, n the density of the gas and c the speed of light. Alternatively, the flux is obstructed on its way to the clouds. At higher z, the results are different (see Sect. 4.1).

**Table 2.** Modelling Leloudas et al (2015) SLSN host spectra. (Line ratios to H$\beta$ =1)

| | z | [OII] 3727+ | [OIII] 4363 | [OIII] 5007+ | Hα 6563 | [NII] 6584 | $V_s$ km s$^{-1}$ | $n_0$ cm$^{-3}$ | $D$ $10^{18}$ cm | Hβ flux$^1$ | O/H $10^{-4}$ | N/H $10^{-4}$ | $T_*$ $10^4$K | $U$ - |
|---|---|---|---|---|---|---|---|---|---|---|---|---|---|---|
| SN1999as R | 0.127 | 9.14 | - | 4.5 | 5.5 | 1.5 | - | - | - | - | - | - | - | - |
| ml1 | | 8.8 | 0.37 | 4.67 | 4.5 | 2 | 200 | 50 | 1.43 | 0.00014 | 2.2 | 0.6 | - | - |
| mll1 | | 8.4 | 0.05 | 4.5 | 3. | 1.8 | 350 | 110 | 1.6 | 1.67 | 7.3 | 0.5 | 30 | 0.2 |
| SN as loc | 0.127 | <2.54 | - | 5.84 | 3.68 | <0.38 | - | - | - | - | - | - | - | - |
| ml2 | | 2. | 0.34 | 6.1 | 3.2 | 0.2 | 760 | 110 | 0.87 | 0.0016 | 2 | 0.05 | - | - |
| mll2 | | 1.98 | 0.017 | 6.0 | 2.94 | 0.42 | 250 | 100 | 2. | 0.084 | 5. | 0.3 | 5 | 0.1 |
| SN1999bd II | 0.151 | 3.4 | - | 2. | 4.64 | 1.44 | - | - | - | - | - | - | - | - |
| ml3 | | 3.3 | 0.16 | 2. | 4.1 | 1.7 | 250 | 40 | 4.4 | 0.0002 | 1.2 | 0.6 | - | - |
| mll3 | | 3.2 | 0.005 | 1.98 | 3. | 0.64 | 210 | 90 | 100 | 0.1 | 6.6 | 0.3 | 3.8 | 0.1 |
| SN2006oz I | 0.396 | 3.7 | - | 5. | 3.47 | <1.3 | - | - | - | - | - | - | - | - |
| ml4 | | 3.9 | 0.2 | 4.6 | 3. | 0.22 | 740 | 230 | 0.4 | 0.012 | 5.1 | 0.04 | - | - |
| mll4 | | 3.5 | 0.012 | 4.87 | 3. | 0.68 | 220 | 90 | 100 | 0.1 | 6.4 | 0.3 | 5 | 0.1 |
| SN2006tf II | 0.074 | 4. | - | 3.68 | 4.37 | 0.4 | - | - | - | - | - | - | - | - |
| ml5 | | 4.2 | 0.2 | 3.43 | 3. | 0.4 | 600 | 220 | 0.24 | 0.01 | 6.6 | 0.08 | - | - |
| mll5 | | 4.4 | 0.053 | 3.54 | 3.9 | 0.8 | 340 | 120 | 1.6 | 1.27 | 5. | 0.2 | 4 | 0.6 |
| SNLS06D4eu I | 1.588 | 2.33 | - | 5.0 | 2.32 | 0.24 | - | - | - | - | - | - | - | - |
| ml6 | | 2.3 | 0.36 | 5.23 | 3.46 | 0.28 | 540 | 190 | 0.243 | 0.002 | 2. | 0.05 | - | - |
| mll6 | | 2.2 | 0.074 | 5.3 | 3.3 | 0.46 | 350 | 120 | 25. | 24.3 | 0.8 | 0.06 | 10. | 0.1 |
| SN2007bi R | 0.128 | 3.2 | - | 4.17 | 3.27 | 0.2 | - | - | - | - | - | - | | |
| ml7 | | 3.3 | 0.23 | 4.0 | 3.1 | 0.39 | 650 | 75 | 1 | 0.02 | 3.6 | 0.1 | - | - |
| mll7 | | 3.2 | 0.026 | 4.17 | 2.94 | 0.4 | 240 | 130 | 0.4 | 0.026 | 3. | 0.1 | 7.3 | 0.02 |
| SN2008am II | 0.233 | 3.12 | - | 3. | 4. | 0.56 | - | - | - | - | - | - | - | - |
| ml8 | | 3. | 0.22 | 3. | 3.2 | 0.76 | 500 | 200 | 0.22 | 0.0045 | 3.9 | 0.2 | - | - |
| mll8 | | 3. | 0.019 | 3.1 | 3. | 0.75 | 240 | 130 | 0.4 | 0.026 | 3. | 0.2 | 6.3 | 0.02 |
| PTF09cnd I | 0.258 | 4.12 | - | 4.53 | 3.44 | 0.28 | - | - | - | - | - | - | - | - |
| ml10 | | 3.9 | 0.2 | 4.6 | 3. | 0.34 | 740 | 230 | 0.4 | 0.012 | 5.1 | 0.06 | - | - |
| mll10 | | 4.5 | 0.024 | 4.53 | 3. | 0.65 | 240 | 130 | 0.4 | 0.026 | 5.9 | 0.2 | 6.3 | 0.02 |
| 2010gx I | 0.230 | 1.19 | 0.21 | 6.56 | 3.7 | 0.057 | - | - | - | - | - | - | - | - |
| ml11 | | 1.04 | 0.45 | 6.87 | 3. | 0.24 | 900 | 570 | 0.21 | 0.02 | 6.2 | 0.1 | - | - G |
| mll11 | | 1.1 | 0.15 | 6.9 | 2.9 | 0.1* | 330 | 200 | 0.16 | 0.57 | 2.4 | 0.1 | 21 | 0.3 |
| 2010kd R | 0.101 | 1.01 | 0.16 | 6.46 | 3.05 | 0.09 | - | - | - | - | - | - | - | - |
| ml12 | | 1.04 | 0.45 | 6.87 | 3. | 0.24 | 900 | 570 | 0.21 | 0.02 | 6.2 | 0.1 | - | - |
| mll12 | | 1.1 | 0.15 | 6.9 | 2.9 | 0.1* | 330 | 200 | 0.16 | 0.57 | 2.4 | 0.1 | 21 | 0.3 |
| PTF10hgi I | 0.099 | 7.98 | - | 6.66 | 7.08 | 1.08 | - | - | - | - | - | - | - | - |
| ml13 | | 7.2 | 0.4 | 7.4 | 3.1 | 1. | 650 | 70 | 1.1 | 0.0016 | 6.3 | 0.2 | - | - |
| mll13 | | 8.2 | 0.082 | 6.77 | 4.3 | 1.2 | 340 | 120 | 1.6 | 1.63 | 7.2 | 0.3 | 60 | 0.6 |
| PS1-10bzj | 0.649 | 0.98 | 0.07 | 8.21 | - | - | - | - | - | - | - | - | - | - |
| ml14 | | 1.2 | 0.44 | 8.13 | - | - | 770 | 560 | 0.174 | 0.016 | 5.6 | 0.1 | - | - |
| mll14 | | 0.97 | 0.17 | 7.8 | 2.9 | 0.1 | 330 | 210 | 0.16 | 0.58 | 2.6 | 0.1 | 21 | 0.4 |
| PTF10heh II | 0.338 | 2. | - | 3.58 | 2.4 | 0.15 | - | - | - | - | - | - | - | - |
| ml15 | | 1.8 | 0.26 | 3.7 | 3.35 | 0.42 | 540 | 190 | 0.29 | 0.0028 | 2. | 0.1 | | |
| mll15 | | 2. | 0.0067 | 3.32 | 3.0 | 0.3 | 280 | 90 | 10 | 0.23 | 5.8 | 0.3 | 3.7 | 0.42 |
| PTF10qaf II | 0.284 | 1.8 | - | 0.81 | 4.55 | 1.47 | - | - | - | - | - | - | - | - |
| ml16 | | 1.4 | 0.05 | 0.95 | 3. | 1.35 | 790 | 120 | 0.9 | 0.013 | 2. | 0.3 | - | - |
| mll16 | | 1.7 | 0.003 | 0.88 | 3. | 1.77 | 210 | 90 | 100 | 0.092 | 3.9 | 0.9 | 3.4 | 0.1 |
| qaf SN loc | 0.284 | 2.7 | - | 2.36 | 2. | 0.6 | - | - | - | - | - | - | - | - |
| ml17 | | 3.1 | 0.1 | 2.2 | 2.96 | 0.6 | 700 | 220 | 0.39 | 0.02 | 5.0 | 0.2 | - | - |
| mll17 | | 2.7 | 0.016 | 2.47 | 2.94 | 0.75 | 240 | 130 | 0.4 | 0.026 | 2.7 | 0.2 | 5.9 | 0.02 |
| PTF10vqv I | 0.452 | 1.3 | 0.09 | 6.33 | 1.87 | 0.8 | - | - | - | - | - | - | - | - |
| ml18 | | 1.36 | 0.4 | 6.89 | 3.2 | 0.62 | 760 | 110 | 0.86 | 0.0013 | 2. | 0.3 | | |
| mll18 | | 1.24 | 0.097 | 6.8 | 3.2 | 0.59 | 346 | 260 | 7. | 64.5 | 0.9 | 0.1 | 5. | 0.1 |
| SN2011ke I | 0.143 | 0.98 | 0.113 | 5.67 | 2.9 | <0.033 | - | - | - | - | - | - | | |
| ml19 | | 0.98 | 0.39 | 6.2 | 3.2 | 0.4 | 730 | 220 | 0.43 | 0.0028 | 2. | <0.2 | | |
| mll19 | | 1.3 | 0.09 | 6.3 | 3.29 | 0.07 | 350 | 300 | 1 | 14.3 | 0.95 | 0.01 | 5 | 0.1 |
| tadpole | 0.143 | 5.06 | - | 4.67 | 3.58 | <0.04 | - | - | - | - | - | - | - | - |
| ml20 | | 4.9 | 0.34 | 5.1 | 3.2 | 0.57 | 500 | 200 | 0.176 | 0.0036 | 5. | <0.1 | | |
| mll20 | | 5.2 | 0.07 | 4.7 | 3.78 | 0.12 | 340 | 120 | 0.16 | 1.37 | 7.4 | 0.04 | 40 | 0.6 |
| SN2011kf I | 0.245 | 1.85 | - | 6.1 | 3.5 | <0.38 | - | - | - | - | - | - | - | - |
| ml21 | | 2. | 0.34 | 6.1 | 3.2 | 0.39 | 760 | 110 | 0.87 | 0.0016 | 2 | 0.1 | - | - |
| mll21 | | 1.98 | 0.017 | 6.0 | 2.94 | 0.42 | 250 | 100 | 2. | 0.084 | 5. | 0.3 | 5 | 0.1 |
| PS1-11ap R | 0.524 | 3.13 | - | 4.8 | - | - | - | - | - | - | - | - | - | - |
| ml22 | | 3.9 | 0.2 | 4.7 | 3. | 0.22 | 740 | 230 | 0.4 | 0.012 | 5.1 | 0.4 | - | - |
| mll22 | | 3.4 | 0.012 | 4.88 | 3. | 0.68 | 220 | 90 | 100 | 0.1 | 6.5 | 0.3 | 5 | 0.1 |
| PTF11dsf II | 0.385 | 2.68 | - | 4.9 | 2.9 | <0.15 | - | - | - | - | - | - | - | - |
| ml23 | | 2.4 | 0.26 | 5.2 | 3.46 | 0.3 | 540 | 190 | 0.24 | 0.002 | 8. | 0.1 | - | - |
| mll23 | | 2.5 | 0.068 | 5.0 | 3.3 | 0.32 | 350 | 100 | 25. | 14.0 | 0.8 | 0.04 | 10. | 0.1 |
| SN2012il I | 0.175 | 1.27 | 0.13 | 7.7 | 3.0 | <0.1 | - | - | - | - | - | - | - | - |
| ml24 | | 1.24 | 0.43 | 8.1 | 3. | 0.15 | 770 | 560 | 0.18 | 0.016 | 5.6 | 0.05 | - | - |
| mll24 | | 1.11 | 0.16 | 7.44 | 2.93 | 0.15 | 330 | 200 | 0.16 | 0.57 | 2.6 | 0.1 | 21 | 0.3 |
| PTF12dam R | 0.107 | 1.54 | 0.08 | 7.8 | 3.5 | 0.19 | - | - | - | - | - | - | - | - |
| mll25 | | 1.56 | 0.1 | 7.3 | 3.3 | 0.4 | 350 | 300 | 1 | 14.3 | 1.1 | 0.06 | 5 | 0.1 |
| SSS120810 I | 0.156 | 2.7 | - | 2.88 | 3. | < 0.24 | - | - | - | - | - | - | - | - |
| ml26 | | 2.7 | 0.11 | 2.4 | 3 | 0.4 | 730 | 220 | 0.39 | 0.02 | 5.3 | 0.05 | - | - |
| mll26 | | 2.8 | 0.018 | 2.8 | 2.94 | 0.38 | 240 | 130 | 0.4 | 0.026 | 2.8 | 0.1 | 6.1 | 0.02 |

$^1$ in erg cm$^{-2}$ s$^{-1}$

### 3.5 LGRB host galaxy spectra from the Savaglio et al (2009) sample

We have selected from the sample of LGRB host galaxy spectra presented by Savaglio et al (2009) the objects showing enough lines to constrain the models (Table 7). Comparing the results for the O/H relative abundances obtained by Savaglio et al by different methods and by detailed modelling confirms that significant differences can lead to different conclusions about the LGRB host galaxy nature. As mentioned in Sect. 2 the main theoretical reason of the gap derives from the fact that the lines within a galaxy are emitted from gas in various physical conditions. Detailed modelling was used to explain the conditions in local galaxies where the spectra account for many lines in different ionization levels and corresponding to many elements. We believe that the same models should be used for galaxies at higher redshifts even if at the state of the art the lines are few.

### 3.6 LGRB host galaxies with different characteristics

The modelling of the host spectra of GRB 980425 presented by Sollerman et al (2005), GRB 991108 presented by both Castro-Tirado et al. (2001) and Graham & Fruchter (2013), GRB 010921, GRB 011121, 020819B, GRB 050824, GRB 050826 and GRB 070612A by Graham & Fruchter (2013), GRB051022 by Levesque et al (2010), GRB 091127 by Vergani et al (2011) and GRB 000210 by Piranomonte et al

**Table 3.** Modelling Sanders et al (2008) SN host galaxy spectra. (Line ratios to H$\beta$ =1)

| | z | [OII] 3727+ | [OIII] 4363 | [OIII] 5007+ | H$\alpha$ 6563 | [NII] 6584+ | [SII] 6737+ | $V_S$ km s$^{-1}$ | $n_0$ cm$^{-3}$ | $D$ $10^{18}$ cm | H$\beta$ flux[1] | O/H $10^{-4}$ | N/H $10^{-4}$ | S/H $10^{-4}$ | $T_*$ $10^4$K | $U$ - |
|---|---|---|---|---|---|---|---|---|---|---|---|---|---|---|---|---|
| **Type**:IIb | | | | | | | | | | | | | | | | |
| 2007ea | 0.04 | 4.15 | - | 3.3 | 3.0 | 0.65 | 0.74 | - | - | - | - | - | - | - | - | - |
| msnd1 | | 4.1 | - | 3.23 | 2.95 | 0.68 | 0.8 | 300 | 120 | 0.5 | 0.02 | 6.6 | 0.23 | 0.05 | 6. | 0.025 |
| 2010am | 0.02 | 2.97 | - | 3.94 | 3.0 | 0.64 | 1.14 | - | - | - | - | - | - | - | - | - |
| msnd2 | | 3.0 | - | 4.0 | 2.9 | 0.66 | 1.18 | 300 | 120 | 0.5 | 0.027 | 5.6 | 0.26 | 0.07 | 6.2 | 0.04 |
| 2010cn | 0.026 | 3.0 | - | 3.94 | 2.7 | 0.27+ | 0.68 | - | - | - | - | - | - | - | - | - |
| msnd3 | | 3.0 | - | 4.0 | 2.9 | 0.53 | 0.69 | 300 | 120 | 0.5 | 0.028 | 5.2 | 0.2 | 0.04 | 6.2 | 0.04 |
| **Type**:Ib | | | | | | | | | | | | | | | | |
| 2006ja | 0.077 | 4.5 | - | 3.1 | 3.1 | 2.45 | 1.02 | - | - | - | - | - | - | - | - | - |
| msnd4 | | 4.3 | - | 3.1 | 3.0 | 2.4 | 0.9 | 300 | 100 | 0.5 | 0.014 | 6.6 | 0.8 | 0.05 | 6.3 | 0.02 |
| 2007az | 0.035 | 2.15 | - | 5.26 | 2.6 | 0.18 | 0.52 | - | - | - | - | - | - | - | - | - |
| msnd5 | | 2.2 | - | 5.16 | 2.9 | 0.21 | 0.53 | 200 | 100 | 0.5 | 0.027 | 6.2 | 0.13 | 0.03 | 6.1 | 0.07 |
| 2007gg | 0.038 | 3.1 | - | 3.4 | 3.5 | 0.8+ | 1.9 | - | - | - | - | - | - | - | - | - |
| msnd6 | | 3.1 | - | 3.5 | 3.0 | 1. | 1.7 | 300 | 120 | 0.5 | 0.024 | 5.6 | 0.4 | 0.1 | 6.2 | 0.033 |
| 2008gc | 0.049 | 2.9 | - | 3.0 | 3.2 | 0.56 | 0.89 | - | - | - | - | - | - | - | - | - |
| msnd7 | | 3.1 | - | 3.1 | 3.0 | 0.58 | 0.85 | 320 | 120 | 0.6 | 0.025 | 5.0 | 0.2 | 0.05 | 6.0 | 0.033 |
| LSQ11JW | 0.02 | 3.0 | - | 2.0 | 2.6 | 0.44+ | 0.4+ | - | - | - | - | - | - | - | - | - |
| msnd8 | | 3.1 | - | 2.0 | 2.9 | 0.5 | 0.7 | 300 | 100 | 0.6 | 0.032 | 6.0 | 0.2 | 0.05 | 4.9 | 0.032 |
| PTF09dfk | 0.016 | 1.97 | - | 4.2 | 3.0 | 0.53 | 1.08 | - | - | - | - | - | - | - | - | - |
| msnd9 | | 2.0 | - | 4.26 | 3.0 | 0.51 | 0.96 | 200 | 100 | 0.5 | 0.027 | 6.2 | 0.34 | 0.06 | 5.7 | 0.07 |
| **Type:Ic** | | | | | | | | | | | | | | | | |
| 2004ib | 0.056 | 11.5 | - | 2.87 | 3.0 | 0.7 | 1.12 | - | - | - | - | - | - | - | - | - |
| msnd10 | | 11.6 | - | 2.8 | 3.1 | 0.75 | 1.27 | 370 | 130 | 0.1 | 0.007 | 7.0 | 0.1 | 0.04 | 15. | 0.006 |
| 2006ir | 0.021 | 2.25 | - | 3.33 | 3.0 | 0.42 | 0.72 | - | - | - | - | - | - | - | - | - |
| msnd11 | | 2.3 | - | 3.4 | 2.9 | 0.42 | 0.78 | 200 | 100 | 0.5 | 0.023 | 6.2 | 0.25 | 0.05 | 5.4 | 0.05 |
| 2007db | 0.048 | 7.3 | - | 2.9 | 3.0 | 0.79 | 1.27 | - | - | - | - | - | - | - | - | - |
| msnd12 | | 7.2 | - | 2.98 | 3.0 | 0.8 | 0.92 | 350 | 130 | 0.1 | 0.01 | 6.2 | 0.15 | 0.04 | 9.0 | 0.01 |
| 2007hl | 0.056 | 8.84 | - | 1.2 | 3.0 | 1.1 | 1.1 | - | - | - | - | - | - | - | - | - |
| msnd13 | | 8.3 | - | 1.2 | 3.2 | 0.8 | 1.7 | 380 | 110 | 0.3 | 0.006 | 8.0 | 0.1 | 0.03 | 14. | 0.0016 |
| 2008ao | 0.015 | 1.42 | - | 0.47 | 3.0 | 1.34 | 0.36 | - | - | - | - | - | - | - | - | - |
| msnd14 | | 1.7 | - | 0.47 | 3.0 | 1.0 | 0.84 | 320 | 150 | 1.5 | 0.05 | 6.0 | 0.5 | 0.1 | 3.5 | 0.058 |
| 2010Q | 0.054 | 2.12 | 0.10 | 6.4 | 2.6 | 0.22 | 0.73 | - | - | - | - | - | - | - | - | - |
| msnd15 | | 2.2 | 0.02 | 6.47 | 2.94 | 0.22 | 0.74 | 200 | 100 | 0.5 | 0.037 | 6.6 | 0.15 | 0.04 | 6.6 | 0.09 |
| msnd15-0 | | 2.2 | 0.08 | 6.7 | 3.0 | 0.21 | 0.8 | 200 | 100 | 2.4 | 0.037 | 4. | 0.12 | 0.03 | 6.3 | 0.055 |
| 2011it | 0.051 | 2.6 | - | 1.43 | 3.6 | 1.45 | 1.65 | - | - | - | - | - | - | - | - | - |
| mnd16 | | 2.5 | - | 1.5 | 3.0 | 1.4 | 1.3 | 250 | 100 | 0.5 | 0.02 | 6.3 | 0.7 | 0.1 | 4.5 | 0.035 |
| PTF10bip | 0.051 | 3.93 | - | 3.35 | 3.4 | 0.52 | 1.18 | - | - | - | - | - | - | - | - | - |
| msnd17 | | 3.91 | - | 3.48 | 3.0 | 0.6 | 1.04 | 300 | 100 | 0.5 | 0.017 | 6.0 | 0.22 | 0.06 | 6.2 | 0.026 |
| **Type:Ic-BL** | | | | | | | | | | | | | | | | |
| 2006nx | 0.137 | 6.0 | - | 4.7 | 2.9 | 0.55 | 1.13 | - | - | - | - | - | - | - | - | - |
| msnd18 | | 6.0 | - | 4.75 | 2.9 | 0.53 | 1.13 | 300 | 100 | 0.5 | 0.019 | 6.6 | 0.14 | 0.06 | 7.9 | 0.017 |
| 2007ce | 0.046 | 1.19 | 0.098 | 7.5 | 2.7 | 0.99 | 0.26 | - | - | - | - | - | - | - | - | - |
| msnd19* | | 1.1 | 0.096 | 7.1 | 3.0 | 0.7 | 0.2 | 150 | 60 | 0.98 | 0.025 | 8.0 | 1.5 | 0.3 | 5.5 | 0.08 |
| 2008iu | 0.130 | 0.86 | 0.2 | 8.3 | 3.0 | 0.3 | 0.17+ | - | - | - | - | - | - | - | - | - |
| msnd20* | | 2. | 0.67 | 7.7 | 3.5 | 1. | 0.06 | 800 | 450 | 0.003 | 0.005 | 5. | 0.4 | 0.2 | 0.8 | 0.01 |
| 2010ah | 0.05 | 3.8 | - | 2.4 | 3.5 | 0.33+ | 0.13 | - | - | - | - | - | - | - | - | - |
| msnd21 | | 3.8 | - | 2.9 | 3.0 | 0.6 | 0.8 | 300 | 120 | 0.5 | 0.002 | 6.6 | 0.23 | 0.05 | 5.4 | 0.02 |
| 2010ay | 0.067 | 2.33 | 0.046 | 7.52 | 2.5 | 0.33 | 0.51 | - | - | - | - | - | - | - | - | - |
| msnd22* | | 2.0 | 0.069 | 6.1 | 2.97 | 0.3 | 0.47 | 200 | 100 | 2.4 | 0.034 | 4.5 | 0.2 | 0.2 | 6.3 | 0.055 |
| **Type:undet. Ibc** | | | | | | | | | | | | | | | | |
| 1991R | 0.035 | 8.38 | - | 2.2 | 3.0 | 0.96 | 1.09 | - | - | - | - | - | - | - | - | - |
| msnd23 | | 8.3 | - | 2.2 | 3.0 | 0.9 | 1.0 | 360 | 120 | 0.1 | 0.006 | 6.2 | 0.15 | 0.04 | 6.3 | 0.006 |
| 2011gh | 0.018 | 3.38 | - | 0.57 | 3.0 | 1.35 | 0.88 | - | - | - | - | - | - | - | - | - |
| msnd24 | | 3.4 | - | 0.56 | 3.0 | 1.39 | 0.9 | 200 | 100 | 1.5 | 0.007 | 6.4 | 0.5 | 0.06 | 4.2 | 0.007 |

[1] in erg cm$^{-2}$ s$^{-1}$

**Table 4.** Modelling Modjaz et al (2008) Type Ic (broad-line) selected host galaxy central spectra

| z | SN 2005kr 0.1345 | | SN 2005ks 0.0987 | | SN 2006nx 0.1370 | | SN 2006qk 0.0584 | |
|---|---|---|---|---|---|---|---|---|
| line ratios | obs | mM1 | obs | mM2 | obs | mM3 | obs | mM4 |
| [OII]3727+ | 1.67 | 1.9 | 2.97 | 2.72 | 3.11 | 3.2 | 3.54 | 3.3 |
| H$\gamma$ | 0.37 | 0.46 | - | - | - | - | 0.43 | 0.46 |
| H$\beta$ | 1 | 1 | 1 | 1 | 1 | 1 | 1 | 1 |
| [OIII]5007+ | 4.0 | 4.1 | 0.92 | 0.88 | 3.85 | 3.3 | 0.33[2] | 0.6 |
| HeI 5876 | 0.14 | 0.15 | - | - | - | - | - | - |
| [OI]6300+ | 0.13 | 0.13 | 0.11 | 0.29 | - | - | - | - |
| [NII]6563+ | 0.38 | 0.4 | 1.4 | 1.5 | 0.25 | 0.47 | 1.6 | 1.53 |
| H$\alpha$ | 3.46 | 3 | 3 | 3 | 3 | 3 | 3 | 3 |
| [SII]6717 | 0.54 | 0.50 | 0.71 | 0.63 | - | - | 0.75 | 0.65 |
| [SII]6731 | 0.34 | 0.9 | 0.52 | 0.86 | - | - | 0.45 | 0.1 |
| $V_S$ (kms) | - | 300 | - | 140 | - | 300 | - | 300 |
| $n_0$ (cm$^{-3}$) | - | 220 | - | 180 | - | 110 | - | 90 |
| $D$ ($10^{16}$cm) | - | 8 | - | 100 | - | 5 | - | 20 |
| $T_*$ ($10^4$K) | - | 5.4 | - | 5.2 | - | 5.4 | - | 4.2 |
| $U$ | - | 0.09 | - | 0.009 | - | 0.041 | - | 0.01 |
| O/H ($10^{-4}$) | - | 6.2 | - | 6.0 | - | 6.2 | - | 4.6 |
| N/H ($10^{-4}$) | - | 0.2 | - | 0.6 | - | 0.2 | - | 0.6 |
| S/H ($10^{-4}$) | - | 0.13 | - | 0.1 | - | 0.3 | - | 0.13 |
| H$\beta$ (erg cm$^{-2}$ s$^{-1}$) | 8.2[1] | 0.091 | 69.6[1] | 0.019 | 6.9[1] | 0.027 | 43.7[1] | 0.0073 |

[1] $\times 10^{-17}$

[2] only the 5007 component was observed

(2015) is shown in Table 8. The models are given in Table 9. Sollerman et al (2005) spectrum was selected because the survey refer to low redshift galaxies (z< 0.2) that host GRB. They claim that they are star-forming galaxies (L< $L_\odot$ ) with relatively low metallicity. The spectra include the He I 5876 line which is also significant in SN Type 1c hosts relatively to WR stars. Sollerman et al derived for the first time the SFR of the GRB 980425 host. They have shown that this galaxy is not very metal-poor, and that a population study based on the broad-band photometry is consistent with a normal star forming galaxy with continuous star formation over 5 - 7 Gyrs, i.e., not with a starburst galaxy. A similar

**Table 5.** Modelling Modjaz et al (2008) Type Ic (broad-line) host observed spectra at SN positions

| | SN 1997ef | | SN 2003jd | | SN 2005kz | | SN 2005nb | |
|---|---|---|---|---|---|---|---|---|
| z | 0.0117 | | 0.0188 | | 0.0270 | | 0.0238 | |
| line ratios | obs | mM5 | obs | mM6 | obs | mM7 | obs | mM8 |
| [OII]3727+ | 2.3 | 2.5 | 3.13 | 3.3 | 0.51 | 0.55 | 3.11 | 3.86 |
| [NeIII]3869+ | - | - | 0.08 | 0.087 | - | - | - | - |
| Hγ | 0.42 | 0.46 | 0.43 | 0.46 | - | - | 0.5 | 0.46 |
| Hβ | 1 | 1 | 1 | 1 | 1 | 1 | 1 | 1 |
| [OIII]5007+ | 0.57 | 0.57 | 2. | 2.1 | *0.175 | 0.18 | 1.6 | 1.56 |
| [OI]6300+ | - | - | 0.057 | 0.057 | 0.24 | 0.2 | - | - |
| [NII]6563+ | 0.82 | 0.87 | 0.53 | 0.58 | 1.98 | 1.0 | 0.76 | 0.79 |
| Hα | 3. | 3. | 3.28 | 3. | 2.53 | 3.6 | 3. | 3. |
| [SII]6717 | 0.52 | 0.5 | 0.48 | 0.4 | - | - | 0.25 | 0.27 |
| [SII]6731 | 0.4 | 0.7 | 0.4 | 0.5 | - | - | 0.24 | 0.36 |
| $V_s$ (kms) | - | 160 | - | 160 | - | 170 | - | 160 |
| $n_0$ ($cm^{-3}$) | - | 130 | - | 120 | - | 220 | - | 120 |
| $D$ ($10^{16}$cm) | - | 6 | - | 4 | - | 1000 | - | 3 |
| $T_*$ ($10^4$K) | - | 3.8 | - | 5 | - | 6 | - | 4.9 |
| $U$ | - | 0.015 | - | 0.015 | - | 0.008 | - | 0.01 |
| O/H ($10^{-4}$ | - | 6.6 | - | 6.6 | - | 5.6 | - | 6.6 |
| N/H ($10^{-4}$ | - | 0.4 | - | 0.25 | - | 1.5 | - | 0.3 |
| S/H ($10^{-4}$ | - | 0.1 | - | 0.1 | - | 0.1 | - | 0.07 |
| Hβ (erg $cm^{-2}$ $s^{-1}$) | 478[1] | 0.013 | 229[1] | 0.011 | 656[1] | 0.097 | 376[1] | 0.008 |

[1] $\times 10^{-17}$

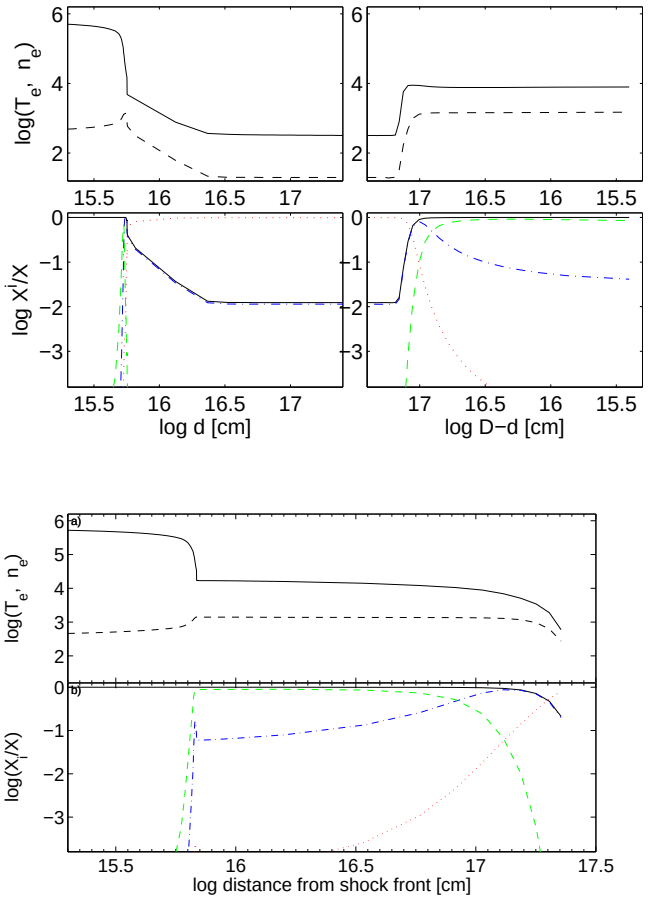


**Figure 2.** Top diagrams refer to the outflow case for model msnd15 (see text). The shock front is on the left and the radiation flux reaches the opposite (right) cloud edge. The bottom diagram refers to the inflow case for model msnd15-0. The shock front is on the left and the radiation flux reaches the same edge at the left of the cloud. Top panels : the profile of the electron temperature (solid line) and the electron density (dashed line) throughout the gas emitting clouds. Bottom panels ; the profiles of $O^{++}/O$ (dashed), $O^+/O$ (dot-dashed, $O^0/O$ (dotted) and $H^+/H$ (solid).

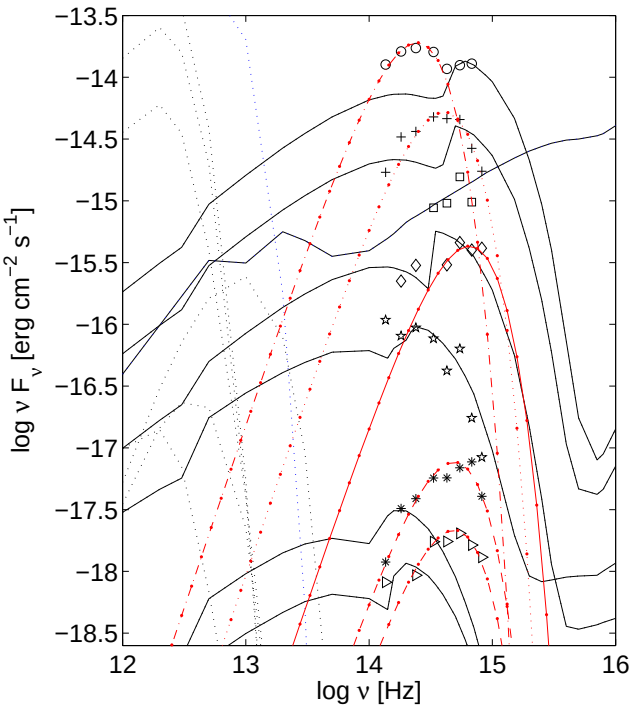


**Figure 3.** The continuum SEDs of LGRB with WR stars (Han et al). Open circles:980703; plus:990712; open squares:020405; open diamonds:030329; open stars: 031203; asterisks:060218; open triangles: 060505b. Solid lines : the bremsstrahlung calculated for each galaxy by models mh1-mh8b. Dotted lines : dust reprocessed radiation. Black body flux calculated by T=8 $10^3$K (solid line + points), by T=6 $10^3$K (dashed line + points), by T=5 $10^3$K (dotted line + points), T=3 $10^3$K (dash-dotted line + points) (see text).

investigation of the spatially resolved H II region where the GRB occurred gives us an estimate of the GRB progenitor mass of $\geqslant 30$ $M_\odot$ consistent with theoretical scenarios of SN 1998bw which lead to a very massive star (e.g. Iwamoto et al. 1998). We have found for 980425 $V_s$ =120km $s^{-1}$and and $n_0$=150 $cm^{-3}$, O/H close to solar and Ne/H solar, but low

**Table 6.** Modelling Krüler et al (2015) long GRB host galaxy spectra. (Line ratios to H$\beta$ =1)

| | z | [OII] 3727+ | [NeIII] 3869 | H$\gamma$ 4360 | [OIII] 5007+ | H$\alpha$ 6563 | [NII] 6584 | $V_s$ km s$^{-1}$ | $n_0$ cm$^{-3}$ | $D$ $10^{18}$cm | H$\beta$ flux$^1$ | O/H $10^{-4}$ | N/H $10^{-4}$ | Ne/H $10^{-4}$ | $T_*$ $10^4$K | $U$ - |
|---|---|---|---|---|---|---|---|---|---|---|---|---|---|---|---|---|
| 050416A | 0.654 | 5.757 | 0.4 | 0.623 | 3.254 | 3.0 | 0.353 | 121 | | | | | | | | |
| mk1 | | 5.9 | 0.67 | 0.46 | 3.85 | 2.95 | 0.46 | 150 | 100 | 0.4 | 0.009 | 6.6 | 1.3 | 1. | 7.0 | 0.008 |
| 050714B | 2.44 | 9.5 | 0.4 | 1.7 | 2.3 | 3. | 1.23 | 96 | | | | | | | | |
| mk2 | | 9.1 | 0.5 | 0.46 | 2.44 | 3. | 1.13 | 100 | 100 | 1. | 0.003 | 6.6 | 0.22 | 0.5 | 11 | 0.002 |
| 050915A | 2.527 | 1.66 | - | 0.28 | 2.17 | - | 210. | - | - | - | - | - | - | - | - | - |
| mk3 | | 2.0 | 0.1 | 0.46 | 2.15 | 2.9 | 0.34 | 230 | 120 | 2. | 0.19 | 4.8 | 0.2 | 1. | 3.6 | 0.2 |
| 050824 | 0.828 | 1.57 | 0.72 | 0.40 | 9.8 | 3.0 | 0.13 | 123.6 | | | | | | | | |
| mk4 | | 1.8 | 0.77 | 0.46 | 9.76 | 3. | 0.117 | 200 | 150 | 8 | 0.114 | 6.5 | 0.1 | 1 | 7. | 0.09 |
| 06111A | 0.76 | 1.67 | 0.33 | - | 5.67 | - | 0.33 | 88.5 | - | - | - | - | - | - | - | - |
| mk5 | | 1.5 | 0.34 | - | 5.67 | - | 0.27 | 70. | 120 | 1 | 0.041 | 4.8 | 0.3 | 0.7 | 5. | 0.047 |
| 060814 | 1.9 | 3.537 | 0.0 | 0.0 | 4.67 | 3.0 | 0.0 | 314 | | | | | | | | |
| mk6 | | 3.3 | 0.2 | 0.46 | 4.6 | 2.9 | 0.3 | 280 | 80 | 0.4 | 0.053 | 6.6 | 0.2 | 0.7 | 4.5 | 0.07 |
| 061021 | 0.34 | 3.99 | 0.0 | 0.443 | 4.06 | 3.0 | 0.158 | 62.7 | | | | | | | | |
| mk7 | | 3.7 | - | 0.46 | 4.15 | 2.93 | 0.25 | 80 | 100 | 0.7 | 0.008 | 5.1 | 0.1 | 1. | 6.2 | 0.008 |
| 061202 | 2.25 | 3.83 | 0.0 | 0.0 | 3.64 | 3.0 | 0.29 | 158.8 | | | | | | | | |
| mk8 | | 3.8 | - | - | 3.7 | 2.95 | 0.25 | 150 | 100 | 1.3 | 0.018 | 6.4 | 0.1 | 1. | 6.2 | 0.014 |
| 070110 | 2.35 | 1.97 | 0.114 | 0.641 | 7.63 | 3.0 | 0.86 | 75.5 | | | | | | | | |
| mk9 | | 1.6 | 0.21 | 0.46 | 7.55 | 2.9 | 0.83 | 75 | 120 | 1 | 0.04 | 6.2 | 1. | 0.4 | 5.6 | 0.047 |
| 070129 | 2.34 | 3.65 | 0.63 | 0.55 | 5.4 | 3.0 | 0.33 | 185 | | | | | | | | |
| mk10 | | 3.9 | 0.7 | 0.45 | 5.2 | 3.1 | 0.57 | 200 | 150 | 8 | 0.083 | 6.3 | 0.2 | 0.9 | 7.3 | 0.033 |
| 070224 | 1.99 | 7.5 | 2.5 | 0.83 | 12.5 | - | - | 100 | - | - | - | - | - | - | - | - |
| mk11 | | 8. | 2.06 | 0.46 | 12.7 | 3. | - | 100 | 100 | 0.2 | 0.007 | 6.7 | 0.3 | 1.3 | 12. | 0.008 |
| 070306 | 1.5 | 2.17 | 0.228 | 0.793 | 5.0 | 3.0 | 0.359 | 289 | | | | | | | | |
| mk12 | | 1.9 | 0.26 | 0.45 | 5.14 | 3.3 | 0.64 | 280 | 150 | 1 | 0.17 | 6.5 | 0.5 | 0.5 | 7. | 0.05 |
| 070318 | 0.84 | 1.677 | 0.233 | 0.241 | 5.316 | 3.0 | 0.273 | 134 | | | | | | | | |
| mk13 | | 1.9 | 0.27 | 0.46 | 5.21 | 2.94 | 0.13 | 130 | 100 | 1 | 0.05 | 6.2 | 0.12 | 0.8 | 4.8 | 0.062 |
| 070328 | 2.06 | 1.1 | 0.45 | 0.09 | 2.45 | - | - | 224 | - | - | - | - | - | - | - | - |
| mk14 | | 1.1 | 0.25 | 0.46 | 2.3 | - | - | 220 | 190 | 7 | 0.78 | 4. | 0.12 | 2. | 3.5 | 0.9 |
| 070419B | 1.96 | 2.439 | 0.0 | 0.0 | 3.030 | 3.0 | 0.0 | 208 | | | | | | | | |
| mk15 | | 2.22 | 0.11 | 0.46 | 3.0 | 2.9 | 0.15 | 210 | 120 | 0.8 | 0.4 | 6. | 0.12 | 1. | 3.5 | 0.5 |
| 070802 | 2.45 | 2.916 | 0.246 | 0.311 | 4.582 | 3.0 | 0.709 | 143 | | | | | | | | |
| mk16 | | 2.7 | 0.26 | 0.46 | 4.5 | 2.9 | 0.67 | 140 | 100 | 1 | 0.037 | 6.2 | 0.4 | 0.7 | 5.2 | 0.03 |
| 071021 | 2.45 | 1.2 | 0.11 | 0.25 | 2.57 | 3.2 | 0.0 | 240.7 | - | - | - | - | - | - | - | - |
| mk17 | | 1.7 | 0.09 | 0.45 | 2.51 | 2.95 | 0.29 | 240 | 250 | 1. | 1.3 | 6.0 | 0.2 | 1. | 3.3 | 1.2 |
| 080207 | 2.086 | 2.028 | 0.73 | 1.2 | 4.836 | 3.0 | 0.68 | 324 | | | | | | | | |
| m18 | | 1.8 | 0.5 | 0.46 | 4.9 | 3.2 | 0.52 | 320 | 80 | 1.1 | 0.084 | 6.6 | 0.5 | 1. | 9.7 | 0.04 |
| 080605 | 1.64 | 2.77 | - | - | 5.0 | 3. | 0.4 | 194 | | | | | | | | |
| m19 | | 2.76 | 0.26 | 0.46 | 5.2 | 2.94 | 0.34 | 200 | 80 | 1. | 0.037 | 6.6 | 0.22 | 0.7 | 5. | 0.05 |
| 080804 | 2.2 | 1.25 | 0.97 | 0.0 | 5.8 | 3.0 | 0.0 | 127.9 | - | - | - | - | - | - | - | - |
| mk20 | | 1.2 | 0.6 | - | 5.9 | 3. | - | 130 | 100 | 0.8 | 0.086 | 6.6 | 0.6 | 1.5 | 6.3 | 0.08 |
| 080805 | 1.5 | 2.6 | 0.0 | 0.0 | 2.485 | 3.0 | 0.226 | 136 | | | | | | | | |
| mk21 | | 2.73 | - | - | 2.63 | 3. | 0.4 | 130 | 100 | 1.2 | 0.03 | 6.6 | 0.2 | 1.5 | 7.8 | 0.01 |
| 081210 | 2.06 | 1. | 0.38 | 0.52 | 2.86 | - | - | 282 | - | - | - | - | - | - | - | - |
| mk22 | | 1.1 | 0.26 | 0.45 | 2.84 | - | - | 280 | 100 | 10 | 0.2 | 6.8 | 0.6 | 1.7 | 4.5 | 0.15 |
| 081221 | 2.26 | 1.143 | 0.0 | 0.0 | 1.884 | 3.0 | 0.409 | 225 | | | | | | | | |
| mk23 | | 1.1 | - | - | 1.92 | 3.27 | 0.46 | 230 | 180 | 25 | 0.29 | 6. | 0.6 | 1. | 4.8 | 0.07 |
| 090201 | 2.1 | 2.099 | 0.203 | 0.697 | 2.050 | 3.0 | 0.055 | 405.8 | | | | | | | | |
| mk24$_{OS}$ | | 1. | 0.3 | 0.44 | 2.5 | 3.8 | 0.4 | 400 | 400 | 0.2-20 | 0.003 | 1. | 0.2 | 0.3 | - | - |
| mk46$_0$ | | 1.5 | 0.37 | 0.45 | 1.9 | 3.3 | 0.17 | 400 | 300 | 2 | 0.0072 | 3. | 0.1 | 0.4 | 9. | 0.001 |
| mk25$_{AGN}$ | | 1.2 | 0.27 | 0.46 | 2.3 | 3. | 0.23 | 400 | 250 | 0.12 | 0.66 | 6. | 0.1 | 0.8 | 4$^2$ | - |
| 090407 | 1.448 | 3.744 | 0.518 | 0.192 | 1.286 | 3.0 | 0.748 | 261.5 | | | | | | | | |
| mk26 | | 3.7 | 0.73 | 0.45 | 1.35 | 3.18 | 0.98 | 260 | 120 | 1 | 0.015 | 5. | 0.3 | 1.4 | 7. | 0.008 |
| 090926B | 1.24 | 6.911 | 0.648 | 0.331 | 6.220 | 3.0 | 0.274 | 161 | | | | | | | | |
| mk27 | | 6.5 | 0.7 | 0.46 | 6.1 | 2.9 | 0.39 | 160 | 110 | 0.8 | 0.024 | 6.6 | 0.1 | 0.7 | 9. | 0.01 |
| 091018 | 0.97 | 2.624 | 0.0 | 0.0 | 3.838 | 3.0 | 0.932 | 143 | | | | | | | | |
| mk28 | | 2.7 | - | 0.46 | 3.86 | 2.9 | 0.9 | 140 | 120 | 1.4 | 0.037 | 6.6 | 0.5 | 0.7 | 5.3 | 0.037 |
| 091127 | 0.49 | 5.321 | 0.209 | 0.466 | 6.495 | 3.0 | 0.219 | 86.5 | | | | | | | | |
| mk29 | | 4.7 | 0.29 | 0.46 | 6.5 | 2.93 | 0.25 | 80 | 120 | 0.8 | 0.011 | 6.6 | 0.1 | 0.4 | 7. | 0.009 |
| 100316D | 0.059 | 2.83 | 0.323 | 0.476 | 5.300 | 3.0 | 0.175 | - | | | | | | | | |
| mk30* | | 2.8 | 0.36 | 0.46 | 5.5 | 2.94 | 0.33 | 140 | 100 | 1 | 0.03 | 6.6 | 0.2 | 0.8 | 5.6 | 0.003 |
| 100418A | 0.623 | 3.907 | 0.160 | 0.482 | 3.450 | 3.0 | 0.349 | 140 | | | | | | | | |
| mk31 | | 3.7 | 0.26 | 0.46 | 3.5 | 2.94 | 0.47 | 140 | 100 | 1 | 0.018 | 6.6 | 0.2 | 0.7 | 5.6 | 0.015 |
| 100424A | 2.47 | 1.887 | 0.748 | .414 | 8.403 | 3.0 | 0.0 | 211 | | | | | | | | |
| mk32 | | 1.9 | 0.6 | 0.46 | 8.4 | 2.9 | 0.25 | 210 | 150 | 1.5 | 0.112 | 5. | 0.2 | 0.7 | 6. | 0.085 |
| 100615A | 1.4 | 4.984 | 0.590 | 0.245 | 8.883 | 3.0 | 0.375 | 117 | | | | | | | | |
| mk33 | | 5. | 0.66 | 0.46 | 8.6 | 2.9 | 0.54 | 120 | 100 | 0.8 | 0.014 | 6.8 | 0.2 | 0.7 | 8.4 | 0.013 |
| 100621A | 0.543 | 2.047 | 0.274 | 0.425 | 4.608 | 3.0 | 0.179 | 199.5 | | | | | | | | |
| mk34 | | 2.5 | 0.3 | 0.46 | 4.6 | 2.97 | 0.37 | 200 | 150 | 2 | 0.075 | 5. | 0.2 | 0.7 | 5. | 0.05 |
| 100814A | 1.44 | 1.826 | 0.555 | 0.0 | 5.743 | 3.0 | 0.223 | 88.5 | | | | | | | | |
| mk35 | | 1.74 | 0.43 | - | 5.79 | 2.93 | 1.2 | 90 | 150 | 0.8 | 0.068 | 6.6 | 0.2 | 1.2 | 5. | 0.057 |
| 100816A | 0.8 | 10.213 | 0.851 | 0.0 | 0.880 | 3.0 | 1.064 | 266 | | | | | | | | |
| mk36 | | 8.7 | 0.8 | - | 1.18 | 3.5 | 1.0 | 270 | 70 | 1.3 | 0.003 | 7.4 | 0.2 | 0.5 | 28. | 0.002 |
| 110818A | 3.36 | 2.75 | 0.38 | - | 9.2 | - | - | 215 | - | - | - | - | - | - | - | - |
| mk37 | | 2.5 | 0.6 | - | 9.1 | - | - | 220 | 130 | 7 | 0.084 | 6.6 | 0.4 | 0.8 | 7. | 0.06 |
| 110918A | 0.984 | 2.29 | 0.245 | 0.0 | 0.9 | 3.0 | 1.007 | 300.9 | | | | | | | | |
| mk38 | | 1.9 | 0.2 | 0.44 | 0.87 | 3.3 | 1.0 | 300 | 90 | 0.7 | 0.03 | 6.6 | 0.8 | 0.9 | 7.5 | 0.0095 |

[1] in erg cm$^{-2}$ s$^{-1}$; [2] in $10^{10}$ photons cm$^{-2}$ s$^{-1}$ eV$^{-1}$ at the Lyman limit

N/H and S/H similar to other galaxies at this z. The SB effective temperature is 6.5 $10^4$ K higher than Sollerman et al results. The FWHM of the line profiles observed by Castro-Tirado et al and reported in Table 3 for 991208 are broad (1200 km s$^{-1}$). The spectrum shows only a few lines, but the model is constrained by the high velocity shock. O/H is slightly lower than solar, but Ne/H and N/H are solar. In contrast, the spectrum reported by Graham & Fruchter shows $V_s$ similar to those which appear for other LGRB hosts in the other surveys. For both models mGRB2a and mGRB2b $U$ is higher than generally found. The FWHM of 091127 host observed by Vergani et al are rather narrow (50 km s$^{-1}$). The [OII]/H$\beta$ line ratio is unusually high. The modelling shows low $V_s$ and $n_0$ (60 km s$^{-1}$and 60 cm$^{-3}$, respectively), very thin clouds (0.03 pc) and O/H 1.12 solar, while N/H and S/H are low. Piranomonte et al present VLT/X-Shooter spectra of the LGRB hosts at z< 2. We have selected GRB 000210 host galaxy spectrum from the Piranomonte et al (2015) sample because both the H$\alpha$ and H$\beta$ lines were measured. Our modelling leads to "normal" parameters (mGRB11). For all the LGRB hosts presented in Table 8 O/H is close to solar.

Table 6 - continued

| | z | [OII] 3727+ | [NeIII] 3869 | Hγ 4360 | [OIII] 5007+ | Hα 6563 | [NII] 6584 | $V_s$ km s$^{-1}$ | $n_0$ cm$^{-3}$ | $D$ $10^{18}$ cm | Hβ flux[1] | O/H $10^{-4}$ | N/H $10^{-4}$ | Ne/H $10^{-4}$ | $T_*$ $10^4$K | $U$ - |
|---|---|---|---|---|---|---|---|---|---|---|---|---|---|---|---|---|
| 111209A | 0.677 | 4.04 | 0.479 | 0.455 | 5.604 | 3.0 | 0.246 | 96.4 | | | | | | | | |
| mk39 | | 4.2 | 0.37 | 0.46 | 5.6 | 3. | 0.23 | 120 | 100 | 0.7 | 0.015 | 6.6 | 0.1 | 0.6 | 6.4 | 0.014 |
| 120119A | 1.73 | 0.425 | 0.200 | 0.348 | 0.0 | 3.0 | 0.406 | 250 | | | | | | | | |
| mk40 | | 0.35 | 0.2 | 0.45 | 2 | 3. | 0.4 | 300 | 200 | 2. | 1.66 | 6.6 | 1. | 1.4 | 5. | 0.3 |
| 120422A | 0.283 | 6.171 | 0.223 | 0.481 | 2.505 | 3.0 | 0.447 | 77 | | | | | | | | |
| mk41 | | 6.2 | 0.5 | 0.46 | 2.5 | 3. | 0.5 | 80 | 100 | 1. 7 | 0.004 | 6.67 | 0.15 | 1. | 7. | 0.003 |
| 120624B | 2.197 | 3.434 | 0.437 | 0.0 | 7.644 | 3.0 | 0.786 | 188 | | | | | | | | |
| mk42 | | 4. | 0.49 | 0.46 | 7.8 | 2.9 | 0.74 | 200 | 100 | 1.3 | 0.032 | 6.6 | 0.3 | 0.6 | 7. | 0.03 |
| 120714B | 0.398 | 3.92 | 0.44 | 0.2 | 3.96 | 3.0 | 0.240 | 94.4 | | | | | | | | |
| mk43 | | 4.2 | 0.44 | 0.46 | 4.0 | 2.94 | 0.27 | 100 | 120 | 1. | 0.013 | 6.3 | 0.1 | 0.8 | 6.5 | 0.009 |
| 120722A | 0.959 | 3.067 | 0.166 | 0.327 | 3.827 | 3.0 | 0.383 | 141 | | | | | | | | |
| mk44 | | 3.1 | 0.24 | 0.46 | 4. | 3. | 0.45 | 140 | 100 | 3. | 0.024 | 6.3 | 0.2 | 0.5 | 6.5 | 0.016 |
| 120815A | 2.36 | 1.5 | 0.91 | 0.0 | 7.12 | 3.0 | 0.37 | 82.7 | | | | | | | | |
| mk45 | | 1.4 | 0.7 | 0.46 | 7.3 | 2.9 | 0.38 | 80 | 100 | 1. | 0.038 | 6.6 | 0.6 | 1.5 | 5.4 | 0.056 |
| 121024A | 2.3 | 1.552 | 0.0 | 0.0 | 6.228 | 3.0 | 0.305 | 213.2 | | | | | | | | |
| mk46 | | 1.53 | 0.24 | 0.46 | 5.8 | 3. | 0.23 | 200 | 120 | 0.6 | 0.3 | 6.9 | 0.4 | 1. | 4. | 0.6 |
| 130427A | 0.34 | 4.253 | 0.0 | 0.06 | 1.537 | 3.0 | 0.3 | 106.6 | | | | | | | | |
| mk47 | | 4.24 | 0.3 | 0.46 | 1.69 | 3. | 0.28 | 100 | 100 | 1.37 | 0.007 | 6.6 | 0.1 | 1. | 5.7 | 0.005 |
| 130925A | 0.3483 | 3.302 | 0.143 | 0.601 | 1.956 | 3.0 | 0.65 | 126 | | | | | | | | |
| mk48 | | 3.7 | 0.2 | 0.46 | 1.97 | 3. | 0.67 | 130 | 100 | 1.3 | 0.012 | 6.6 | 0.26 | 0.8 | 5.4 | 0.009 |
| 131103A | 0.596 | 1.7 | 0.234 | 0.28 | 4.511 | 3.0 | 0.155 | 200 | | | | | | | | |
| mk49 | | 1.8 | 0.2 | 0.46 | 4.4 | 2.94 | 0.15 | 200 | 130 | 1. | 0.23 | 6.6 | 0.15 | 1. | 4. | 0.28 |
| 131105A | 1.685 | 8.378 | 1.145 | 0.549 | 2.132 | 3.0 | 0.404 | 132 | | | | | | | | |
| mk50 | | 8.1 | 1.19 | 0.46 | 2.14 | 3.1 | 0.5 | 130 | 150 | 1.5 | 0.009 | 6.6 | 0.1 | 1. | 14. | 0.003 |
| 131231A | 0.64 | 2.22 | 0.302 | 0.67 | 5.894 | 3.0 | 0.3 | 92 | | | | | | | | |
| mk51 | | 2.5 | 0.35 | 0.46 | 5.83 | 2.94 | 0.35 | 100 | 100 | 1. | 0.024 | 6.6 | 0.25 | 0.8 | 5.6 | 0.026 |
| 140301A | 1.41 | 2.92 | 0.0 | 0.386 | 0.953 | 3.0 | 1.032 | 280 | | | | | | | | |
| mk52 | | 2.8 | 0.3 | 0.46 | 1.1 | 3.4 | 0.97 | 280 | 100 | 2.5 | 0.027 | 6.6 | 0.5 | 0.8 | 9. | 0.0078 |

[1] in erg cm$^{-2}$ s$^{-1}$

**Table 7.** Modelling Savaglio et al (2012) long GRB host spectra. (Line ratios to Hβ =1)

| | z | [OII] 3727+ | [NeIII] 3869 | Hγ 4360 | [OIII] 5007+ | Hα 6563 | [NII] 6584 | [SII] 6717 | $V_s$ 1 | $n_0$ 2 | $D$ 3 | Hβ 4 | O/H 5 | N/H 5 | Ne/H 5 | S/H 5 | $T_*$ 6 | $U$ - |
|---|---|---|---|---|---|---|---|---|---|---|---|---|---|---|---|---|---|---|
| 980425[7] | 0.0085 | 2.07 | 0.49 | - | 6.76 | 3 | 0.18 | 0.16 | - | - | - | - | - | - | - | - | - | - |
| ms0 | | 2.0 | 0.5 | - | 6.74 | 3 | 0.18 | 0.19 | 110 | 120 | 0.4 | 0.024 | 6.0 | 0.14 | 0.8 | - | 6.6 | 0.078 |
| 990712 | 0.434 | 2.68 | 0.41 | 0.34 | 6.22 | 3.4 | <0.75 | - | - | - | - | - | - | - | - | - | - | - |
| ms1 | | 2.67 | 0.45 | 0.46 | 6.3 | 2.94 | 0.62 | - | 100 | 100 | 0.5 | 0.012 | 6.6 | 0.4 | 0.8 | - | 7.3 | 0.03 |
| 020903 | 0.251 | 1.9 | 0.44 | 0.35 | 7.23 | 3.6 | 0.08 | 0.2 | - | - | - | - | - | - | - | - | - | - |
| ms2 | | 2.0 | 0.5 | 0.46 | 7.2 | 2.9 | 0.13 | 0.2 | 110 | 120 | 0.4 | 0.024 | 6.0 | 0.1 | 0.8 | 0.02 | 6.8 | 0.079 |
| 030329 | 0.168 | 1.74 | 0.34 | 0.41 | 4.87 | 2.76 | 0.15 | - | - | - | - | - | - | - | - | - | - | - |
| ms3 | | 1.76 | 0.33 | 0.46 | 4.85 | 2.94 | 0.16 | 0.16 | 110 | 120 | 0.4 | 0.024 | 6.0 | 0.14 | 0.85 | 0.02 | 5.6 | 0.078 |
| 031203 | 0.1055 | 0.74 | 0.44 | 0.42 | 8.6 | 2.94 | 0.16 | 0.09 | - | - | - | - | - | - | - | - | - | - |
| ms4 | | 0.94 | 0.5 | 0.46 | 8.54 | 2.91 | 0.17 | 0.09 | 180 | 350 | 0.3 | 0.36 | 5.0 | 0.13 | 0.5 | 0.04 | 6.4 | 1.5 |
| 060218 | 0.0334 | 2.11 | 0.37 | 0.52 | 6.08 | 3.4 | 0.20 | 0.15 | - | - | - | - | - | - | - | - | - | - |
| ms5 | | 2.1 | 0.39 | 0.46 | 6.2 | 2.9 | 0.24 | 0.19 | 100 | 100 | 0.5 | 0.016 | 6.6 | 0.2 | 0.8 | 0.02 | 6.5 | 0.06 |
| 060505 | 0.2889 | 3.6 | - | 0.28 | 2.27 | 3.69 | 0.7 | 0.78 | - | - | - | - | - | - | - | - | - | - |
| ms6 | | 3.5 | - | 0.46 | 2.3 | 3. | 0.75 | 0.73 | 130 | 100 | 1.3 | 0.003 | 6.6 | 0.3 | 0.8 | 0.08 | 6.4 | 0.009 |

[1] in km s$^{-1}$; [2] in cm$^{-3}$ ;[3] in $10^{18}$ cm; [4] in erg; [5] $10^{-4}$; [6] in $10^4$K; [7] reddening corrected;

### 3.7 Han et al (2010) sample of LGRB hosts showing He, Ar and Fe lines

Han et al present the spectra of LGRB hosts with richer data and determine metallicities by direct methods. We present in Table 10 the modelling of Han et al spectra and in Table 11 the models adopted to reproduce the line ratios. Our results were obtained constraining the models on the basis of the He, Ar and Fe lines, which are seldom observed in the SN and GRB host spectra. We have found in the host galaxies shock velocities $\geqslant$ 200 km s$^{-1}$and $n_0$ between 50 and 350 cm$^{-3}$. Ar/H and Fe/H are by factors of 2 and 6 lower than solar, respectively. However, Fe/H is based on one only object, 980703. The O/H abundances calculated by the detailed modelling of the spectra are higher than those calculated by Han et al adopting the direct method (Sect. 4.2). N/H and S/H are lower than solar up to a factor of 10. To best reproduce the spectra of 980703 and 990712 we adopted He/H=0.13. Higher than solar (0.1) He/H are found close to WR stars. In 980703 spectrum the HeII lines were not observed, but a high He/H=0.13 was predicted by modelling. Helium is a strong coolant and affects the calculation of the whole spectrum. The large cloud geometrical thickness reaching ∼30 pc were found by modelling the 060505b spectrum which refers to the entire host. In most of the host galaxies $D \sim 10$ pc, while in 020405 and 060218 $D$ = 0.003 pc and 0.01 pc, respectively. These small clouds have relatively high $n_0$. The models were calculated adopting an inward motion of the clouds, towards the star-forming region. $T_*$ are low, 3 $10^4$ K, but not exceptional. Particularly low are the ionization parameters, indicating that the emitting regions in these two objects are far from the SB stars. The SN associated with 020903 most probably occurred at several hundred parsecs from a bright, relatively compact region responsible for WR and O star traces in the spectrum (Hammer et al 2006). Accordingly, the calculated geometrical thickness of the emitting clouds is relatively large ($D$=3 pc). We find for 031203 O/H solar and for 030329 O/H 0.34 solar. A J-band image presented by Gal-Yam et al. (2004) for 031203 shows that the GRB occurred in the central regions of the host galaxy.

In Fig. 3 we present the modelling of the continuum SED of the Han et al host continuum emission. The observed different object fluxes are shifted along the Y-axis in order to compare the SEDs in the same diagram. The Y-axis scale refers only to 980703. The data were not reddening corrected, therefore the near-UV should be considered as lower limits. For each galaxy we show the bremsstrahlung (black line) calculated by the model which best fits the line spectrum (Table 11), the reprocessed radiation by dust calculated by a dust-to-gas ratio $d/g$=$10^{-15}$ by number (dotted line) and the black body (bb) flux referring to temperatures selected phenomenologically to best fit the SED. Reradia-

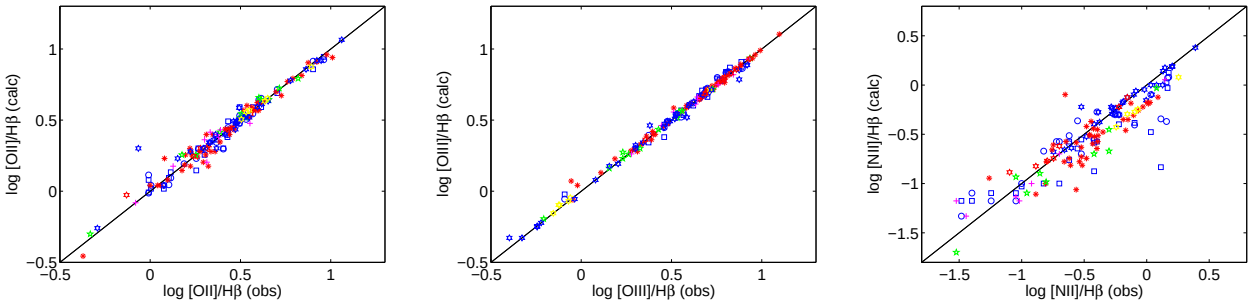


**Figure 4.** Comparison of observed line ratios to H$\beta$ calculated by detailed modelling with the data by Leloudas et al : blue circles (SB models), blue squares (SD models); by Krühler et al : red asterisks; by Sollerman et al , Graham & Fruchter, Vergani et al, and Piranomonte et al : green stars; by de Ugarte Postigo : yellow hexagrams; by Han et al : magenta plus

tion by dust grains are shown only to indicate the peak frequency range. The temperatures referring to the bb fluxes, which range between 3 and 8 $10^3$ K, are by a factor $> 10$ lower than those found for the SB stars by modelling the line spectra. They represent an older stellar population throughout the hosts. Except for 020405 and 031203 which can be reproduced by the bremsstrahlung alone, the other SEDs are well fitted by the summed bremsstrahlung and bb fluxes. For 030329 two bb fluxes at different temperatures are present, while for 990712, 060218 and 060505 the bremsstrahlung plays a negligible role. The latter refers to the whole host.

### 3.8 SGRB 130603B and SGRB 051221A host galaxies

The spectra by FORS2 and X-shooter at VLT and ACAM at WHT were observed by de Ugarte Postigo et al (2014). They claim that SGRB most probably derive from the merger of compact objects, in particular for the short duration GRB 130603B, on the basis of the detection of "kilonova"-like signature associated with Swift. The host galaxy is a perturbed spiral due to interaction with another galaxy (de Ugarte Postigo et al). In the spectrum taken by X-shooter the afterglow dominates the continuum, but the lines emitted from the host were used in their modelling. Therefore, we refer to line ratios and not to line fluxes. The FORS spectra show the core, the arm and the opposite side of the galaxy. We report the X-shooter and FORS reddening corrected spectra observed by de Ugarte Postigo in Table 12, neglecting the GTC spectra because they do not include the H$\alpha$ line. Each observed spectrum is followed by the best fitting model (mS1-mS4) in the next column. The spectrum observed by Cucchiara et al (2013) for SGRB 130603B is also reported in Table 12 for comparison.

The models show shock velocities and pre-shock densities in the norm. However, to best reproduce all the line ratios we adopted a magnetic field $B_0$ higher by a factor of 3 than for the LGRB galaxies presented in the previous sections. A higher $B_0$ prevents compression in the downstream gas, but its effect on the line ratio results is different than that obtained reducing the preshock density (see Contini 2009). We find O/H near solar in all the positions in agreement with de Ugarte Postigo et al results, and N/H and S/H lower than solar by factors $\geqslant 2$. S/H in FORS (OT site) is nearly solar. The cloud geometrical thickness is relatively large ($D$=1.8 pc) in the X-shooter (OT site). $D$=0.3 pc is used to fit the FORS spectra, showing a larger cloud fragmentation. The spectrum reported by Cucchiara et al (2013) is reproduced by model (mS5) similar to those used to fit the spectra observed by de Ugarte Postigo et al. Star temperatures and ionization parameters referring to the SGRB are rather low ($\sim$ 3.5 $10^4$ K and $\sim$ 0.01, respectively).

Most of the spectra presented for SGRB surveys (e.g. Fong et al 2013, Berger et al 2005) do not contain enough line to constrain the models. We report in Table 12, last two columns, the spectrum observed by Soderberg et al (2006) for SGRB 051221a at z=0.546 and model mS6. The line ratios were reddening corrected adopting H$\gamma$/H$\beta$ =0.46. The best fitting model shows 12+log(O/H)=8.8, in agreement with Soderberg et al who calculated 8.7 by the R32 method (upper branch). We have found $T_*$ =8.2 $10^4$K and $U$=0.007. $T_*$ are higher than for SGRB 130603B, where $T_*$ is rather low ($\sim$ 3.5 $10^4$ K). $U$, however, are similar. For both SGRB 130603B and SGRB 051221a the ionization parameters are relatively low, roughly indicating that the host observed positions are far from the star-forming region. Compared with LGRB hosts reported in Table 8, we cannot find any significant difference in the physical conditions of the host, except for a higher magnetic field in 130603B.

## 4 RESULTS

Most of the present work refers to the modelling of the SN and GRB host galaxy line spectra. The results show that to reproduce narrow line spectra the calculations should account for the coupled effect of shocks and radiation from the starburst within the host galaxy. The precision of modelling is given in graphical form for the strongest lines in Fig. 4. For [NII]/H$\beta$ the fit of calculated to observed line ratios is less precise. In fact, at the velocities corresponding to the FWHM observed in the line profiles, the [NII] doublet is blended with the H$\alpha$ line. Therefore, the derived line intensities are more uncertain.

Most of the parameters which partly describe high redshift issues, such as SFR, stellar masses, element abundances, etc. are calculated from the data observed at Earth. On the other hand, modelling results reveal the conditions of gas and dust at the emitting clouds.

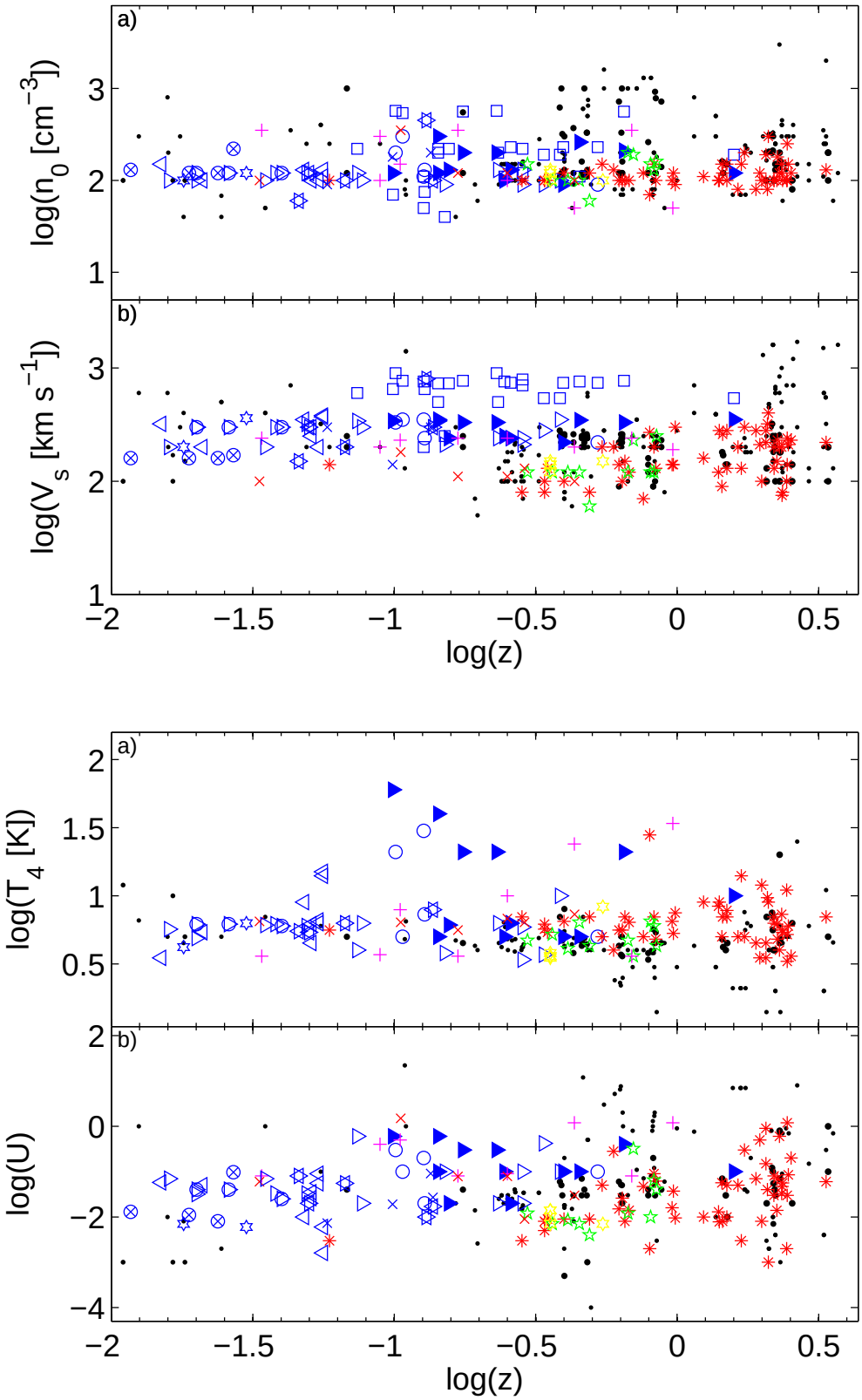


**Figure 5.** Top : $V_s$ and $n_0$ calculated for the galaxy surveys as function of z. Bottom : $T_*$ (in $10^4$K) and $U$. Symbols are described in Table 13.

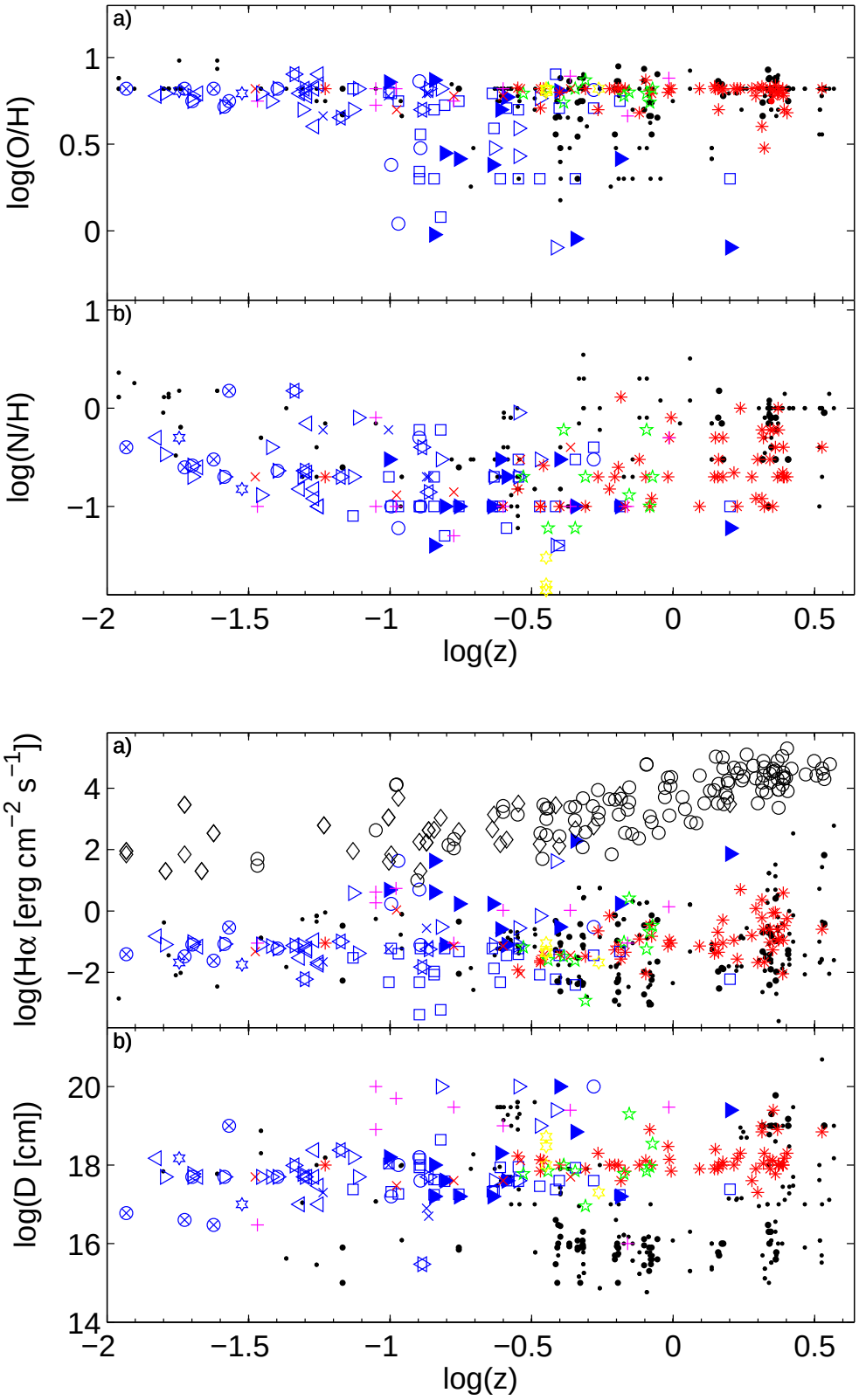


**Figure 6.** Top : O/H and N/H calculated for the galaxy surveys as function of z. Bottom : Hα and $D$. Symbols as in Fig. 5 are described in Table 13. Black open circles and open diamonds : SFR referring to GRB and SN host galaxies, respectively.

**Table 8.** Modelling LGRB hosts from different samples

| | z | [OII] 3727+ | [NeIII] 3689 | Hγ 4360 | [OIII] 5007+ | HeI 5876 | Hα 6563 | [NII] 6583 | [SII] 6726 |
|---|---|---|---|---|---|---|---|---|---|
| 980425[1] | 0.0085 | 4.54 | 0.64 | 0.44 | 3.48 | 0.15 | 2.46 | 0.38 | 0.89 |
| mGRB1 | | 4.4 | 0.6 | 0.46 | 3.63 | 0.18 | 2.95 | 0.3 | 0.7 |
| 991208[2] | 0.7 | 0.466 | - | - | 1.7 | - | - | - | - |
| mGRB2a | | 0.5 | - | - | 1.88 | - | - | - | - |
| 991208[3] | 0.7 | 1.79 | - | - | 2.12 | - | 3. | 0.157 | - |
| mGRB2b | | 1.8 | - | - | 2.0 | - | 3. | 0.156 | - |
| 010921[3] | 0.451 | 5.19 | - | - | 3.4 | - | 3. | 0.14 | - |
| mGRB3 | | 5.3 | - | - | 3.285 | - | 2.95 | 0.19 | - |
| 011121[3] | 0.362 | 4. | - | - | 1.83 | - | 3. | 0.09 | - |
| mGRB4 | | 4.55 | - | - | 1.82 | - | 2.96 | 0.175 | - |
| 020819B[3] | 0.411 | 2.43 | - | - | 0.62 | - | 3. | 1.2 | - |
| mGRB5 | | 2.6 | - | - | 0.64 | - | 2.97 | 1.4 | - |
| 050824[3] | 0.828 | 1.5 | - | - | 8.6 | - | 3. | 0.11 | - |
| mGRB6 | | 1.8 | - | - | 8.61 | - | 2.9 | 0.12 | - |
| 050826[3] | 0.296 | 3.2 | - | - | 1.7. | - | 2.97 | 0.5 | - |
| mGRB7 | | 3.5 | - | - | 1.7 | - | 2.95 | 0.53 | - |
| 051022[4] | 0.806 | 4.12 | 0.29 | 0.46 | 3.62 | - | - | - | - |
| mGRB8 | | 4.4 | 0.34 | 0.46 | 3.67 | - | - | - | - |
| 070612A[3] | 0.671 | 3.16 | - | - | 1.43 | - | 3 | 0.03 | - |
| mGRB9 | | 3.3 | - | - | 1.45 | - | 3 | 0.03 | - |
| 091127[5] | 0.49 | 6.6 | <1.4 | 0.5 | 5.35 | - | 2.75 | <0.5 | 0.75 |
| mGRB10 | | 6.2 | - | 0.46 | 5.2 | - | 3 | 0.32 | 0.06 |
| 000210[6] | 0.846 | 3.37 | 0.136 | 0.37 | 2.68 | - | 2.8 | - | - |
| mGRB11 | | 3.3 | 0.16 | 0.46 | 2.72 | - | 2.94 | - | - |

[1] Sollerman et al(2005); [2] Castro-Tirado et al (2001); [3] Graham & Fruchter (2013); [4] Levesque et al (2010); [5] Vergani et al (2011); [6] Piranomonte et al (2015)

**Table 9.** The models for LGRB hosts in Table 8

| | $V_s$ $km\,s^{-1}$ | $n_0$ $cm^{-3}$ | $D$ $10^{18}cm$ | Hβ $erg\,cm^{-2}\,s^{-1}$ | O/H $10^{-4}$ | N/H $10^{-4}$ | Ne/H $10^{-4}$ | $T_*$ $10^4K$ | $U$ - |
|---|---|---|---|---|---|---|---|---|---|
| mGRB1 | 120 | 150 | 0.65 | 0.0186 | 6.3 | 0.09 | 1. | 6.5 | 0.01 |
| mGRB2a | 1260 | 820 | 0.182 | 0.16 | 6.2 | 1. | 1. | 3 | 0.1 |
| mGRB2b | 230 | 190 | 20. | 0.86 | 6.3 | 0.13 | 1.7 | 3.6 | 0.32 |
| mGRB3 | 120 | 100 | 0.7 | 0.008 | 6.6 | 0.06 | 0.6 | 6.4 | 0.007 |
| mGRB4 | 120 | 100 | 0.7 | 0.0085 | 6.6 | 0.06 | 0.6 | 5.2 | 0.007 |
| mGRB5 | 120 | 100 | 1. | 0.011 | 5.5 | 0.6 | 0.6 | 4.1 | 0.0086 |
| mGRB6 | 120 | 130 | 0.9 | 0.069 | 5.5 | 0.1 | 0.6 | 6. | 0.065 |
| mGRB7 | 120 | 150 | 0.6 | 0.022 | 6.2 | 0.2 | 0.6 | 4.7 | 0.012 |
| mGRB8 | 120 | 150 | 0.7 | 0.0193 | 6.2 | 0.6 | 0.6 | 6.5 | 0.01 |
| mGRB9 | 120 | 200 | 0.6 | 0.032 | 6. | 0.01 | 0.6 | 4.7 | 0.012 |
| mGRB10 | 60 | 60 | 0.09 | 0.0004 | 7.4 | 0.2 | 0.4 | 4.3 | 0.004 |
| mGRB11 | 250 | 160 | 3.5 | 0.11 | 6.6 | 0.2 | 0.6 | 4.3 | 0.04 |

**Table 10.** Modelling Han et al. (2010) host spectra. (Line ratios to Hβ =1)

| | z | [OII] 3727+ | Hγ 4360 | [OIII] 4363 | [FeIII] 4658 | HeII 4686 | [ArIV] 4711+ | [OIII] 5007+ | Hα 6563 | [NII] 6583 | [SII] 6716 | [SII] 6731 |
|---|---|---|---|---|---|---|---|---|---|---|---|---|
| 980703 | 0.966 | 3.57 | 0.46 | - | 0.02 | - | 0.15 | 2.78 | - | - | - | - |
| mh1 | | 3. | 0.42 | - | 0.029 | - | 0.12+ | 2.9 | - | - | - | - |
| 990712 | 0.433 | 2.06 | 0.43 | 0.08 | - | 1.1 | - | 5.73 | 3.75 | <0.036 | - | - |
| mh2 | | 1.6 | 0.45 | 0.083 | - | 1.2 | 0.02 | 5.6 | 3.2 | 0.07 | - | - |
| 020405 | 0.691 | 2.15 | 0.35 | - | - | 0.009 | 0.015 | 4.39 | - | - | - | - |
| mh3[1] | | 2.6 | 0.46 | - | - | 0.01 | 0.011 | 4.4 | 2.9 | - | - | - |
| 020903 | 0.251 | 1.34 | 0.46 | 0.064 | - | 0.045 | 0.14 | 6.96 | 3.03 | 0.09 | 0.25 | 0.15 |
| mh4 | | 1.5 | 0.45 | 0.04 | - | 0.03 | 0.002 | 6.6 | 3.2 | 0.11 | 0.14 | 0.16 |
| 030329 | 0.168 | 2. | 0.45 | 0.072 | - | - | - | 4.3 | 3.16 | 0.03 | 0.39 | 0.2 |
| mh5[1] | | 2.3 | 0.46 | 0.05 | - | - | - | 4.1 | 2.9 | 0.1 | 0.02 | 0.04 |
| 031203 | 0.105 | 0.83 | 0.44 | 0.07 | - | 0.001 | 0.008 | 8.49 | 3.2 | 0.096 | 0.11 | 0.08 |
| mh6 | | 0.83 | 0.46 | 0.05 | - | 0.01 | 0.002 | 8.5 | 3.11 | 0.1 | 0.2 | 0.2 |
| 060218 | 0.034 | 2.45 | 0.46 | 0.05 | - | 0.009 | 0.05 | 4.4 | 2.89 | 0.12 | 0.17 | 0.13 |
| mh7[1] | | 2.7 | 0.46 | 0.05 | - | 0.01 | 0.02 | 4.6 | 2.89 | 0.15 | 0.04 | 0.08 |
| 060505a | 0.089 | 2.35 | 0.43 | - | - | - | - | 3.25 | 3.5 | 0.2 | 0.39 | 0.31 |
| mh8a | | 2.5 | 0.46 | - | - | - | - | 3.6 | 3. | 0.3 | 0.5 | 0.6 |
| 060505b | 0.089 | 2.39 | - | - | - | - | - | 1.9 | 5.6 | 1.4 | 1.25 | 0.66 |
| mh8b | | 2.4 | - | - | - | - | - | 1.83 | 3.1 | 1.7 | 0.6 | 0.7 |

**Table 11.** The models for Han et al (2010) host galaxies in Table 10

| | $V_s$ $km\,s^{-1}$ | $n_0$ $cm^{-3}$ | $D$ $10^{18}cm$ | Hβ $erg\,cm^{-2}\,s^{-1}$ | O/H $10^{-4}$ | N/H $10^{-4}$ | S/H $10^{-4}$ | Ar/H $10^{-4}$ | Fe/H $10^{-4}$ | $T_*$ $10^4K$ | $U$ - |
|---|---|---|---|---|---|---|---|---|---|---|---|
| mh1 | 190 | 50 | 30 | 0.46 | 7.6 | 0.5 | 0.01 | 0.033 | 0.005 | 34 | 1.2 |
| mh2 | 200 | 50 | 25 | 0.35 | 7.8 | 0.1 | 0.01 | 0.033 | 0.005 | 24 | 1.2 |
| mh3 | 240 | 350 | 0.01 | 0.03 | 4.6 | 0.1 | 0.01 | 0.033 | 0.005 | 3.6 | 0.08 |
| mh4 | 240 | 100 | 10 | 0.35 | 6.6 | 0.1 | 0.033 | 0.033 | 0.005 | 10 | 0.09 |
| mh5 | 240 | 350 | 30 | 0.03 | 5.6 | 0.05 | 0.09 | 0.033 | 0.005 | 3.6 | 0.08 |
| mh6 | 230 | 150 | 50 | 1.8 | 6.6 | 0.1 | 0.028 | 0.033 | 0.005 | 7.9 | 0.5 |
| mh7 | 240 | 350 | 0.03 | 0.03 | 5.6 | 0.1 | 0.2 | 0.033 | 0.005 | 3.6 | 0.08 |
| mh8a | 200 | 300 | 8 | 1.39 | 5.3 | 0.1 | 0.04 | 0.033 | 0.005 | 3.7 | 0.4 |
| mh8b | 200 | 100 | 100 | 0.62 | 6.6 | 0.8 | 0.1 | 0.033 | 0.005 | 3.7 | 0.4 |

**Table 12.** Modelling SGRB 130603B at z=0.356 and SGRB 051221a at z=0.546 host galaxy spectra

| line | OT site[1] X-shooter | mS1 | OT site[1] FORS | mS2 | core[1] FORS | mS3 | arm[1] FORS | mS4 | obs[2] | mS5 | 051221a[3] .... | mS6 |
|---|---|---|---|---|---|---|---|---|---|---|---|---|
| [OII]3727+ | 4.47 | 4.5 | 3.4 | 3.6 | 3.55 | 3.7 | 4.3 | 4.3 | 3.05 | 3.2 | 7.8 | 7.5 |
| H$\gamma$ | - | 0.46 | 0.89 | 0.49 | 0.49 | 0.46 | [0.5] | 0.46 | - | 0.46 | 0.46 | 0.46 |
| H$\beta$ | 1 | 1 | 1 | 1 | 1 | 1 | 1 | 1 | 1 | 1 | 1 | 1 |
| [OIII[5007+ | 0.87 | 0.9 | 0.76 | 0.8 | 0.75 | 0.8 | 0.85 | 0.85 | 0.77 | 0.7 | 5.17 | 5.15 |
| H$\alpha$ | 3. | 3. | 3. | 2.96 | 3. | 2.96 | 3. | 3. | 3. | 3. | - | 3. |
| [NII]6585 | 0.7 | 0.76 | 0.57 | 0.56 | 0.85 | 0.85 | 1.8 | 1.8 | 0.78 | 0.8 | - | - |
| [SII]6717 | 0.66 | 0.7 | 1.19 | 1.1 | 0.63 | 0.66 | 0.27 | 0.5 | - | - | - | - |
| [SII]6731 | 0.33 | 0.6 | 0.56 | 0.97 | 0.5 | 0.59 | 0.5 | 0.45 | - | - | - | - |
| $V_s$ (km s$^{-1}$) | - | 140 | - | 150 | - | 150 | - | 140 | - | 120 | - | 150 |
| $n_0$ (cm$^{-3}$) | - | 120 | - | 130 | - | 130 | - | 120 | - | 100 | - | 100 |
| $B_0$ ($10^{-4}$G) | - | 3 | - | 3 | - | 3 | - | 3 | - | 2 | - | 1 |
| $D$ [4] | - | 5.3 | - | 1 | - | 1 | - | 1 | - | 3 | - | 0.2 |
| O/H [5] | - | 6.6 | - | 6.3 | - | 6.3 | - | 6.6 | - | 6.5 | - | 6.6 |
| N/H [5] | - | 0.2 | - | 0.2 | - | 0.3 | - | 0.5 | - | 0.3 | - | 0.13 |
| S/H [5] | - | 0.04 | - | 0.1 | - | 0.06 | - | 0.03 | - | 0.03 | - | 0.03 |
| $T_*$ ($10^4$K) | - | 3.6 | - | 3.5 | - | 3.5 | - | 3.6 | - | 3.8 | - | 8.3 |
| $U$ | - | 0.014 | - | 0.01 | - | 0.01 | - | 0.014 | - | 0.007 | - | 0.007 |
| H$\beta$ [6] | - | 0.014 | - | 0.016 | - | 0.016 | - | 0.03 | - | 0.014 | - | 0.007 |

[1] de Ugarte Postigo et al (2014); [2] Cucchiara et al (2013); [3] Soderberg et al (2006); [4] in $10^{18}$ cm; [5] in $10^{-4}$; [6] in erg cm$^{-2}$ s$^{-1}$

### 4.1 Physical parameters

The results of shock velocities, preshock densities, cloud geometrical thickness, SB effective temperatures, ionization parameters and H$\alpha$ absolute fluxes calculated at the nebula are shown as function of z in Figs. 5 and 6. Fig. 5 top diagram shows the pre-shock densities and the shock velocities calculated in the host clouds. The ranges for SLSN ($n_0$ between 100 and 1000 cm$^{-3}$, and $V_s$ between 100 and 1000 km s$^{-1}$) are similar to those found in local AGN and SB galaxies. The results calculated by RD models are adapted to the expanding shocks resulting from the explosion, propagating through the ISM clouds. $V_s$ upper limits calculated by SD models for the Leloudas et al sample of SLSNII hosts are suitable to the reverse shock. The H$\beta$ fluxes (Table 2) calculated by SD models are relatively low and indicate that they could give only a minimum contribution to the spectra. Velocities of 1000 km s$^{-1}$are characteristic of the Crab nebula SNR. Lower $V_s$ are more appropriated to the older Cygnus Loop SNR filaments. In the redshift range where both LGRB and SN host spectra are observed $V_s$ are higher for the SN hosts. In particular for LGRB hosts, $n_0$ and $V_s$ are located at the lower limit of the ensemble of the data. This suggests that the LGRB event negligibly affects the host galaxy cloud conditions.

Fig. 5 bottom diagram refers to the SB effective temperature and ionization parameter. $T_*$ are relatively high in few SLSNR hosts; in more SLSNI hosts $T_* > 10^5$ K are even higher than in galaxies showing activity at z$\geqslant$ 2. $U$ has a smoother trend. LGRB hosts correspond to relatively low SB temperatures ($\sim 3\ 10^4$K), increasing towards z=2. The same trend is shown for $U$, which appears at the lower limit for 0.4<z< 1.3, it is largely scattered at z> 2, reaching $U \sim$1. Such high $U$ reveal a small dilution factor of the SB flux.

In the bottom diagram of Fig. 6 the cloud geometrical thickness appears as a function of z. Except for a few SLSN where $D$ are close to 3-30 pc, SN and GRB show $D \sim 0.3$ pc for all the host clouds. At z between 0.3 and 2.3, $D$ splits between 0.3 pc for GRB and $D < 0.003$ pc for the other galaxy types. $D$ is obtained phenomenologically by the calculations. It is a leading parameter in modelling because linked with flux absorption and emission in each slab of the downstream gas at different wavelengths. Moreover, $D$ determines the emission measure EM=$\Sigma$ n $n_e$ $\Delta$x, where $\Delta$x is the gas slab thickness ($D$=$\Sigma\Delta$x) and n and $n_e$ the H density and the electron density, respectively in the slabs where the physical conditions are approximately constant. EM enters in the calculations of the line intensities. $D$ depends on fragmentation due to the turbulent regime created by shocks. Blanchard et al (2015) refer to the galaxy sizes, which in compact galaxies could roughly represent the upper limit to the geometrical thickness of the clouds. However, it is generally found that $D$ is small compared with the galaxy dimensions and several clouds are included in each galaxy.

### 4.2 Metallicities

Following Vergani et al, metallicity is one of the main parameters which affects the evolution of massive stars as well as their explosive deaths (e.g. Woosley 1993, etc). In Fig. 6 top diagram we show the results of O/H and N/H calculated in each host by detailed modelling. O/H is depleted in most of the SN and SLSN host clouds for 0.1<z<1, while it is close to solar in most of the GRB hosts. Regarding the N/H ratio, we note a large distribution of N/H from solar to lower than solar by a factor >10 for both SLSN and GRB hosts. Subsolar N/H is an indication of external gas acquisition through merger processes.

In Fig. 7 the results of 12+(O/H)$_d$ calculated for nearby SN Ic hosts by Modjaz et al using Kewley & Dopita (2002) method, SLSN hosts by Leloudas et al. using the Kobulnicky & Kewley (2004) method, SN Type Ibc by Sanders et al using the Zaritsky et al (1994) method, are compared with the results calculated by detailed modelling (12+(O/H)$_m$. Fig. 7 shows that the results for SLSN hosts roughly correlates with those calculated by detailed modelling. The results for the host galaxies of long and short period GRB, LGRB which contain WR stars and other LGRB are neglected because metallicities calculated by detailed modelling are near solar for all of them. Some observed LGRB hosts show high metallicity. Krüler et al (and references therein) point out that "several metal rich GRB were discovered". Graham et al (2015) recently confirmed that high metallicities can be found in LGRB. It was explained by Contini (2014a) that the metallicities in terms of the O/H relative abundances obtained by "direct methods" are lower limits.

Our results about near solar O/H in most LGRB hosts

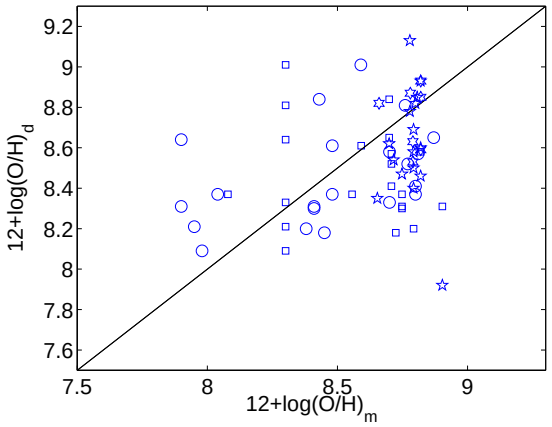


**Figure 7.** Comparison of O/H calculated by detailed modelling (m) with those calculated by direct methods (d) by Leloudas et al : circles (SB models), squares (SD models); by Modjaz et al : hexagrams; by Sanders et al : pentagrams.

are different from those generally obtained by other modelling methods which indicate low metallicities in LGRB galaxy hosts. This leads to serious consequences in evolution theories based on metallicities. We justify our results by claiming that the theoretical calculations of spectral lines and continuum were carefully checked by modelling the rich spectra of local objects. On the other hand, "direct methods" and their results are universally accepted by the scientific community.

### 4.3 SFR, H$\alpha$ line flux and the gas physical parameters

SFR are generally calculated by the observers from the H$\alpha$ luminosity $L_{H\alpha}$ . We will limit our discussion on the SFR, comparing the SFR trend with that of the calculated H$\alpha$ fluxes. The H$\alpha$ flux calculated at the nebula is shown in the bottom diagram (top panel) of Fig. 6. The low H$\alpha$ fluxes calculated by SD models in SLSN host clouds are easily lost in the FWHM sockets of line profiles. The trend of H$\alpha$ for a few SLSNI at lower z is similar to the trend of $T_*$ and $U$ calculated by the RD models, indicating that in the high $T_*$ range the H$\alpha$ fluxes depend on $T_*$ and $U$. We added in the diagram the SFR calculated by the observers for each host galaxy of SN, SLSN (black open diamond) and LGRB (black open circles) surveys shifted by a factor of 1000 for sake of clarity. The increasing trend of SFR with z is clear because it depends on $L_{H\alpha}$ . The increase of H$\alpha$ calculated at the nebula with z is less evident. Fig. 8 diagrams show H$\alpha$ (calculated at the nebula) as function of $T_*$ , $U$, $V_s$ , $n_0$, $D$ and O/H. The top left diagrams indicate that at relatively low SB temperatures ($T_* \leqslant 3\ 10^4$ K), H$\alpha$ fluxes do not increase with $T_*$ and LGRB hosts even show a decreasing trend with SLSNII objects in the top tail. This unexpected trend is due to the effect of the other parameters. At high $T_*$ ($\geqslant 10^5$K) as those found for SLSN host SB, H$\alpha$ increases with $T_*$ . A nearly linear increasing trend of log(H$\alpha$ ) with log($U$) is evident in Fig. 8 top right diagram. H$\alpha$ is a strong function of the ionization parameter $U$, which depends on both the photoionization source (SB) flux and the host cloud density. $T_*$ and $U$ different effects on the calculated line ratios are discussed in Sect. 2.2. The increasing trends of H$\alpha$ with $V_s$ and $n_0$ appear in the middle left and right diagrams, respectively, neglecting SD models for SN. At the relatively low $V_s$ ($< 350$ km s$^{-1}$) and $n_0$ ($< 300$ cm$^{-3}$) which are characteristic of the gas in the host galaxies presented in previous sections, the effect of the other parameters leads to the large scattering of the results. Accordingly, the increasing trend of H$\alpha$ with $D$ (bottom left) is strongly disturbed. The trend of H$\alpha$ with O/H (bottom right) is hardly evident for SLSN hosts which are distributed on a relatively large O/H range. It is even less clear for GRB hosts because most of them show solar O/H.

SFR are calculated by the H$\alpha$ luminosity observed at Earth $L_{H\alpha}$ (Kennicutt 1998). SFR $\propto L_{H\alpha}$ , and $L_{H\alpha}$ =H$\alpha$ (at Earth)$\times$ 4 $\pi$ d$^2$=H$\alpha$ (at the nebula)$\times$ 4 $\pi$ R$^2$ (adopting a filling factor *ff*=1) where d is the distance to Earth and R the radius of the cloud, i.e. the distance of the cloud from the host galaxy SB stars. Fig. 9 shows the results of R as function of z for *ff*=1. The emitting cloud radius in the SLSN hosts are lower than in GRB hosts and in SN hosts at lower z, indicating more compact galaxies. The clouds in SGRB hosts have larger radius than in LGRB hosts at the same z, however, the data are too few to be meaningful. Larger R, best fitting the galaxy observed dimensions, could be found for *ff*$<$ 0.01. It seems from Fig. 9 that the increasing trend of SFR with z at high z depends on R rather than on H$\alpha$ which follows the trend of $U$. New data at higher z are needed.

**Table 13.** The symbols in Figs. 5, 6 and 8

| | |
|---|---|
| blue circles | SLSNR hosts (Leloudas et al) |
| blue open triangles at z$\geqslant$0.1 | SLSNII hosts (Leloudas et al) |
| blue filled triangles | SLSNI hosts (Leloudas et al) |
| blue squares | Shock models for SLSN hosts (Leloudas et al) |
| blue x | Type Ic host central spectra (Modjaz et al) |
| blue encircled x | Type Ic hosts at SN positions (Modjaz et al) |
| blue triangles at z$\leqslant$ 0.1 | SN Ib host (Sanders et al) |
| blue encircled triangles | SN IIb hosts (Sanders et al) |
| blue opposite triangles | SN Ic hosts (Sanders et al) |
| blue double triangles | SN IcBL hosts (Sanders et al) |
| blue hexagrams | SN Ibc (Sanders et al) |
| red asterisks | GRB hosts (Krühler et al) |
| red x | LGRB hosts (Savaglio et al) |
| yellow hexagrams | SGRB hosts (de Ugarte Postigo et al) |
| green pentagrams | LGRB different hosts (Table 8) |
| magenta plus | LGRB hosts with WR stars (Han et al) |
| black dots | other high z galaxies (Contini 2015) |

## 5 CONCLUDING REMARKS

The results obtained by modelling broad lined SN Type Ic hosts by Modjaz et al, SN hosts by Sanders et al and SLSN host galaxies by Leloudas et al are presented in this paper and compared with those calculated for various LGRB and a few SGRB host galaxies at z<3.4. It was found that:

1) The differences between the II , I, and R SLSN types are irrelevant in terms of the host $V_s$ and $n_0$. but $T_*$ and $U$ calculated for a few SLSNI hosts ($> 10^5$K and $\geqslant$0.1, respectively) are higher than for the other SLSN types. The latter are similar to $T_*$ and $U$ calculated for LGRB hosts ($\sim$ 3-7 $10^4$K and 0.01-0.1, respectively).

2) The shock velocities and pre-shock densities in SN host galaxies are similar to those found in the other galaxies reported in Fig. 5, at the same z, but in LGRB hosts they are lower. The $V_s$ calculated by shock dominated models for

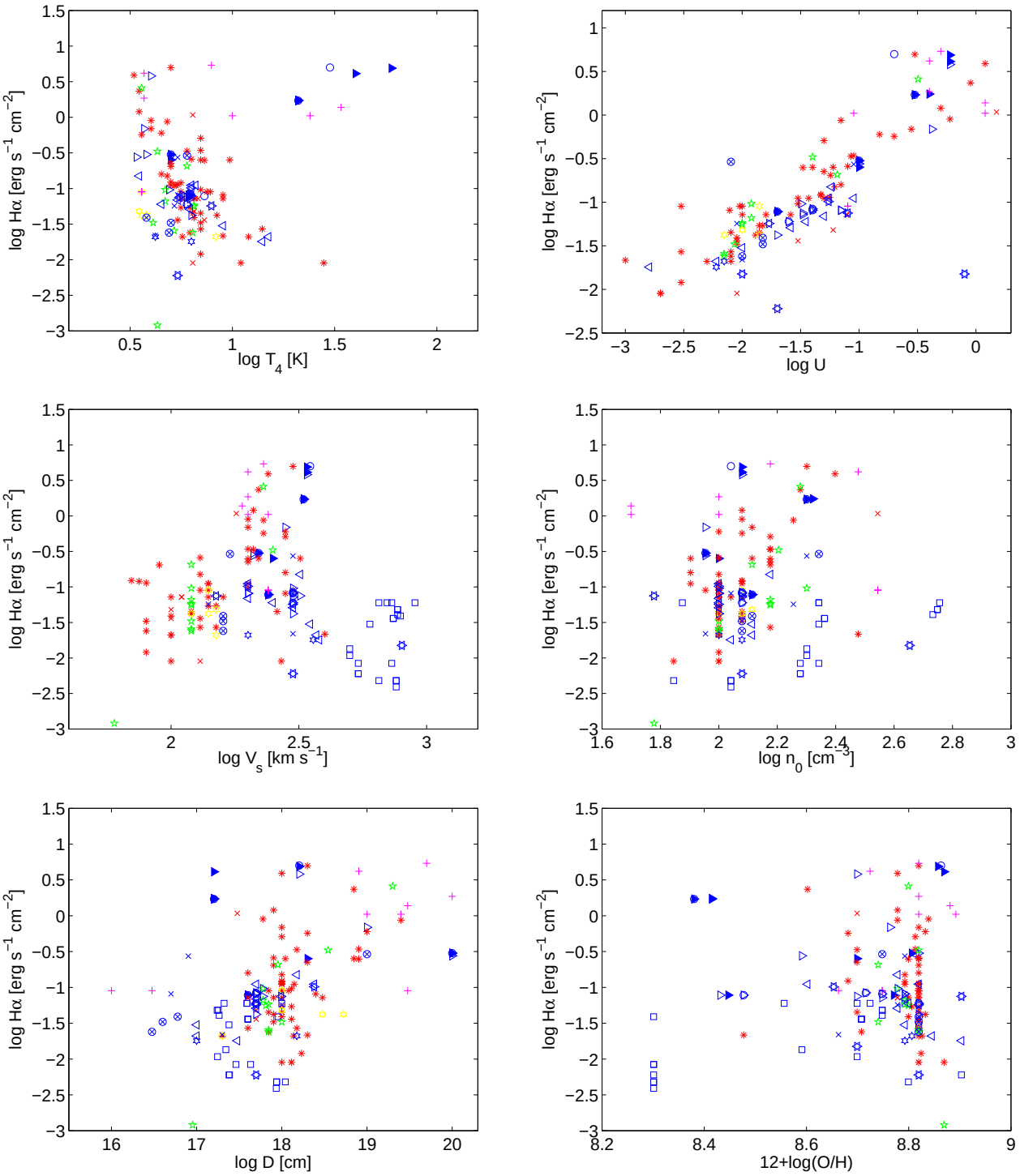


**Figure 8.** Hα as function of the physical parameters. Symbols as in Fig. 5

SLSN hosts are higher than for radiation dominated models, but still lower than those calculated for the Lyα line emitting galaxies at higher z. In the GRB host spectra there is no trace of the high velocity winds predicted by SD models in SLSN host spectra. Such winds would waive the low density extended clouds in the ISM of these hosts.

3) T$_*$ and $U$ calculated for LGRB hosts show that these are rather quiescent galaxies even at z$\sim$ 2. It was found by Contini (2014b) that activity is associated to a high T$_*$ .

4) In SN host galaxies some SB stars have temperatures approaching those of outburst.

5) Models reproducing the line spectra of a sample of LGRB galaxies hosting WR stars (Han et al 2010) at relatively low redshift, show He/H=0.13 in a few objects. Modelling the continuum SED, the contribution of a rather old

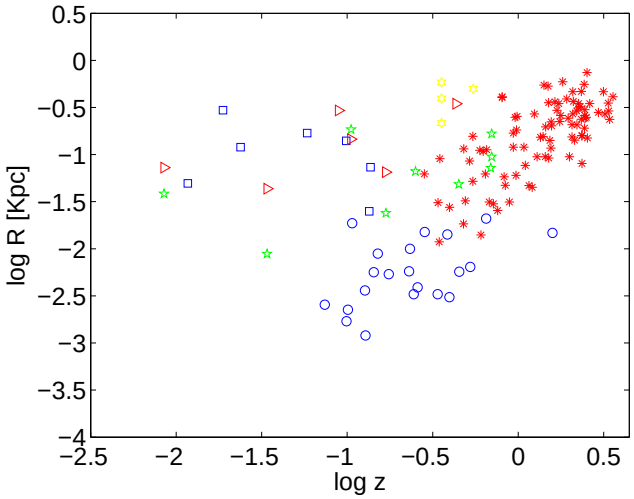


**Figure 9.** The calculated radius of the emitting clouds as a function of redshift. Circles : SLSN (Leloudas et al); squares : SN Type Ic (Modjaz et al); asterisks : LGRB (Krühler et al); triangles :LGRB (Savaglio et al); stars refer to LGRB from surveys including Han et al data; hexagrams : SGRB.

stellar population (3-8 $10^3$ K) appears in the near-IR - optical domain.

6) The O/H relative abundances calculated by detailed modelling of SN hosts are scattered between 12+log(O/H) =8.85 and 8.0. They are close to solar in LGRB hosts, perhaps contaminated by shocked an photoionised gas within the same galaxy. O/H are generally higher than those calculated by "direct methods", in particular for LGRB. N/H are lower than solar by factors of 5-20 for both SN and GRB hosts.

7) The geometrical thickness of the clouds is nearly constant for GRB hosts, $D\sim$ 0.3 pc and shows a small increase at z$\sim$ 2. A uniform $D$ indicates similar turbulent regimes in the ISM of the different hosts. In fact similar shock velocities are found in GRB host clouds.

8) The H$\alpha$ absolute fluxes calculated at the emitting clouds of SLSNI hosts at 0.1< z<0.3, are relatively high, proportionally to $T_*$ and $U$.

9) SLSN host galaxies are more compact than other SN hosts.

Concluding, our analysis of SLSN and GRB host galaxy spectra indicates that some parameters adopted to reproduce the SN and LGRB host galaxy line ratios are different. First, we have found that the velocity field is lower in LGRB host than in SN host galaxies, and it is very similar to that found in SB galaxies. Second, most stars in the SB throughout the SN hosts have reached temperatures similar to those of outburst, indicating that some activity is going on. Moreover, our modelling leads to lower than solar metallicities in term of O/H in SN hosts at 0.1<z<1. Metallicities in LGRB hosts are close to solar throughout the 0.01<z<3.4 range. The present analysis results of SN and GRB host galaxy spectra, in the near UV-optical-far IR range, suggest that the SN-host symbiosis is stronger than the GRB-host one in terms of activity. The physical and chemical conditions in the GRB host galaxies are similar to those in SB galaxies within a large z range.

## ACKNOWLEDGEMENTS

I am very grateful to the referee for critical suggestions which substantially improved the presentation of the paper.

## REFERENCES

Allen, C.W. 1976 Astrophysical Quantities, London: Athlone (3rd edition)
Anders, E., Grevesse, N. 1989, Geochimica et Cosmochimica Acta, 53, 197
Anderson, J.P. et al 2016 arXiv160200011A
Asplund, M., Grevesse, N., Sauval, A.J., Scott, P. 2009, ARAA, 47, 481
Berger, E. et al 2005, Nature, 438, 988
Blanchard, P.K. et al 2015 arXiv:1509.07866
Castro-Tirado, A.J. et al 2001, A&A, 370, 398
Chevalier, R.A. 1982, ApJ, 259, L85
Christensen, L., Vreeswijk, P.M., Sollerman, J. et al 2008, A&A, 490, 45
Contini, M. 2016, submitted
Contini, M. 2015, MNRAS, 452, 3795
Contini, M. 2014b, A&A, 572, 65
Contini, M. 2014a, A&A, 564, 19
Contini, M. 2009, MNRAS, 399, 1175
Contini, M. 2004, A&A, 422, 591
Contini, M. 1987, A&A, 183, 53
Contini, M. , Shaviv, G. 1980 ApSS, 85, 203
Contini, M., Kozlovsky, B.Z., Shaviv, G. 1977, A&A, 59, 387
Cox, D.P. 1972, ApJ, 178, 143
Cucchiara, A. et al. 2013, ApJ, 777,94
de Ugarte Postigo, A. et al 2014, A&A, 563, 62
Fesen, R., Milisavljevic, D. 2015, AAS, 22514024
Filippenko, A. 1997, ARA&A, 35, 309
Fishman, G.J., Meegan, C.A. 1995 ARA&A, 33, 415
Fong, W. et al 2013, ApJ, 769, 56
Fruchter, A.S. et al. 2006, Nature, 441, 463
Gal-Yam, A. et al 2004, ApJ, 609, L59
Graham, J.F. et al 2015 arXiv:1511.00667v
Graham, J.F., Fruchter, A.S. 2013, ApJ, 774, 119
Hammer, F., Flores, H., Schaerer, D., Dessauges-Zavadsky, M., Le Floc'h, E., Puech, M. 2006, A&A, 454, 103
Han, X.H., Hammer, F., Liang, Y.C., Flores, H., Rodrigues, H., Hou, J.L., Wei, J.Y. 2010, A&A, 514, A24
Hjorth, J. et al. 2003, Nature, 423, 847
Iwamoto, K. et al. 1998, Nature, 395, 672
Kann, D.A. et al ApJ, 734, 96
Kennicutt, Jr. R.C. 1998, ARA&A, 36, 189
Kewley, L.J., Dopita, M.A. 2002 ApJS, 142, 35
Kobulnicky, H.A., Kewley, L.J. 2004, ApJ, 617, 240
Kouveliotou, C. et al 1993, ApJ, 413, L101
Kriek, M. et al 2009, ApJ, 700, 221
Krühler, J. et al 2015 A&A, arXiv:1505.06743
Leloudas, G. et al 2015, MNRAS, 574, A61
Levesque, E.M., Berger, E., Kewley, L.J., Bagley, M.M. 2010, ApJ, 139, 694
Maoz, D., Mannucci, F., Nelemans, G. 2014, ARA&A, 52, 107
Modjaz, M. et al 2008, AJ, 135, 1136
Nagao, T., Maiolino, R. , & Marconi, A. 2006, A&A, 459, 85

Osterbrock, D.E. 1974 in 'Astrophysics of Gaseous Nebulae' W.H. Freeman and Company, San Francisco
Paczynski, B. 1998 AIPC, 428, 783
Piranomonte, S. et al 2015, MNRAS, 452, 3293
Rodriguez-Ardila, A., Contini, M., Viegas, S.M. 2005, MNRAS, 357, 220
Rosswog, S.,Ramirez-Ruiz, E., Davies, M.B. 2003, MNRAS, 345,1077
Sanders, N.E. et al. 2012 ApJ, 758, 132
Savaglio, S., Glazerbrook, K., Le Borgne, D. 2009, ApJ, 691, 182
Soderberg, A.M. et al 2006, ApJ, 650, 261
Sollerman J.; Östlin, G.; Fynbo, J. P. U.; Hjorth, J.; Fruchter, A.; Pedersen, K. 2005, NewA, 11, 103
Stanek, K.Z. et al 2003, ApJ, 591, L17
Van Dokkum, P.G., Kriek, M., Rodgers, B., Franx, M., Puxley, P. 2005, ApJ, 622, L16
Vergani, S.D. et al 2011 A&A 535, A127
Williams, R.E. 1967, ApJ, 147, 556
Woosley, S.E. 1993, ApJ, 405, 273
Zaritsky, D., Kennicutt, R.C. Jr, Huchra, J.P. 1994, ApJ, 420, 87